

12-2015

Direct Adaptive Control for Stability and Command Augmentation System of an Air-Breathing Hypersonic Vehicle

Ron Aditya

Follow this and additional works at: <https://commons.erau.edu/edt>



Part of the [Aerodynamics and Fluid Mechanics Commons](#)

Scholarly Commons Citation

Aditya, Ron, "Direct Adaptive Control for Stability and Command Augmentation System of an Air-Breathing Hypersonic Vehicle" (2015). *Dissertations and Theses*. 191.

<https://commons.erau.edu/edt/191>

This Thesis - Open Access is brought to you for free and open access by Scholarly Commons. It has been accepted for inclusion in Dissertations and Theses by an authorized administrator of Scholarly Commons. For more information, please contact commons@erau.edu.

DIRECT ADAPTIVE CONTROL FOR STABILITY AND COMMAND
AUGMENTATION SYSTEM OF AN AIR-BREATHING HYPERSONIC VEHICLE

A Thesis

Submitted to the Faculty

of

Embry-Riddle Aeronautical University

by

Ron Aditya

In Partial Fulfillment of the

Requirements for the Degree

of

Master of Science in Aerospace Engineering

December 2015

Embry-Riddle Aeronautical University

Daytona Beach, Florida

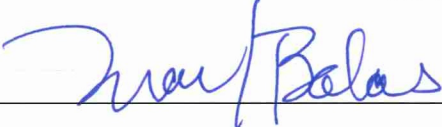
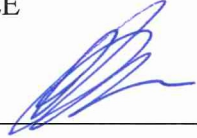
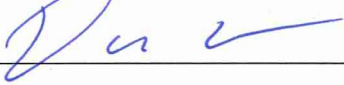

DIRECT ADAPTIVE CONTROL FOR STABILITY AND COMMAND
AUGMENTATION SYSTEM OF AN AIR-BREATHING HYPERSONIC VEHICLE


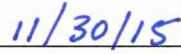
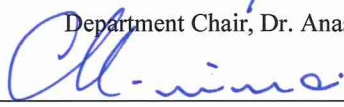
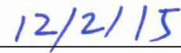
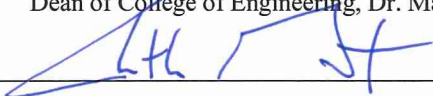
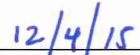
by

Ron Aditya

A Thesis prepared under the direction of the candidate's committee chairman, Dr. Mark J. Balas, Distinguished Professor, Department of Aerospace Engineering, and has been approved by the members of the thesis committee. It was submitted to the School of Graduate Studies and Research and was accepted in partial fulfillment of the requirements for the degree of Master of Science in Aerospace Engineering.

THESIS COMMITTEE

 Chairman, Dr. Mark Balas	 Member, Dr. Bogdan Udrea
 Member, Dr. Darris White	 Member, Dr. Richard Prazenica

 Department Chair, Dr. Anastasios Lyrintzis	 Date
 Dean of College of Engineering, Dr. Maj Mirmirani	 Date
 Vice Chancellor, Academic Support, Dr. Christopher Grant	 Date

ACKNOWLEDGMENTS

I take this opportunity to express my profound gratitude and deep regards to my advisor Dr. Mark J. Balas for his exemplary guidance and for showing a great deal of patience and confidence in my work. Beside my advisor, I would like to thank Dr. Bogdan Udrea and Dr. Kaman S. Thapa Magar for helping me in getting started with this research work.

I would like to thank Dr. Dave Doman at AFRL, WPAB for giving us this opportunity.

I would like to thank my thesis committee member Dr. Darris White for helping us out. I would also like to thank Dr. Richard Prazenica for agreeing to join the committee last minute and providing with necessary feedbacks.

I would like to thank Dr. Andrew Lewis and David Germany at UH for introducing me to Dynamics & Control, a topic that I have been intrigued by and have been interested in, for a few years now.

A special thanks to my family. Words cannot express how grateful I am to my father, mother, and brother for all of the sacrifices that they have made on my behalf. I would also like to thank all of my friends who supported and encouraged throughout my time at ERAU. Last but not the least I would like to thank Mr. Elon Musk, Mr. Jack Ma and Mr. Sundar Pichai for inspiring and motivating me through their work. This work has been supported by AFRL/UTC research contract 14-S2605-04-C24.

Public Release Statement: Cleared for Public Release Case Number: 88ABW-2015-5404.

TABLE OF CONTENTS

1.	INTRODUCTION.....	1
1.1	Hypersonic Flight Background.....	1
1.2	Adaptive Controls Literature Survey.....	3
1.3	Problem Description.....	11
2.	DIRECT ADAPTIVE CONTROL SCHEME.....	15
2.1	System Requirements	21
2.2	Non-Minimum Phase Mitigation.....	22
2.2.1	Zero-relocation.....	22
2.2.2	Minimum Phase Feedback Leakage	24
3.	HSV MODEL AND SIMULATION OVERVIEW	25
3.1	Propulsion.....	26
3.2	Aerodynamics	27
3.3	Structures	27
3.4	Actuator Dynamics	28
3.5	Longitudinal Dynamics	29
3.5.1	Equations of Motion	29
3.5.2	State Variables	30
3.5.3	Control Variables	31
3.5.4	Summary and Conclusion	33
3.6	Simulation Overview	33
4.	ADAPTIVE STABILITY AND COMMAND AUGMENTATION	38
4.1	Linearization.....	38
4.2	Dynamic Properties	41
4.3	Pitch-Axis Stability Augmentation.....	46
4.4	Development of the Pitch-Axis Stability Augmentation.....	48
4.5	Mach-Hold by FER Compensation	52
4.6	Mach-Hold Control Development	53
4.6.1	Simulation Results	54
4.7	Nonlinear System Application.....	58
4.8	Sensor Blending.....	61

5.	MULTIVARIABLE APPROACH.....	64
5.1	Control Scheme in Multivariable Setup	64
5.2	Multivariable Zeros	65
5.2.1	Multivariable Zeros.....	67
5.2.2	Multivariable Transmission Zeros	69
5.3	Multivariable Direct Adaptive Control.....	74
5.4	Coupling Gain Weightings	76
6.	CONCLUSION AND FUTURE WORK.....	82
6.1	Summary.....	82
6.2	Future Work.....	83
7.	REFERENCES	86

LIST OF FIGURES

Figure 1.1: X-51 Mission Profile (Mutzman, et al 2011)	2
Figure 1.2: General Adaptive Controller Structure (Ioannou, et al 2012)	5
Figure 1.3: Principle Structure of Indirect Adaptive Control (Ioannou, et al 2012)	6
Figure 1.4: Design Principle of Direct Adaptive Control (Ioannou, et al 2012)	7
Figure 1.5: Design Principle of MR Direct Adaptive Control (Narendra, et al 2012)	7
Figure 1.6: Error Model Class MRAC Scheme (Wen, et al 1989)	9
Figure 1.7: Error Model Class MRAC Scheme with Persistent Disturbance Rejection (Fuentes, et al 2000)	10
Figure 3.1: Schematic of Hypersonic Scramjet Vehicle (Korad, 2010)	26
Figure 3.2: Schematic of Scramjet Engine (Korad, 2010)	27
Figure 3.3: Hypersonic Vehicle (Bolender, et al 2007)	32
Figure 3.4: Block Diagram Representation of the Nonlinear Model	34
Figure 4.1: Aero Model used for Linearization	40
Figure 4.2: Poles of the Plant	41
Figure 4.3: Zero map of $qs\delta es$	44
Figure 4.4: Zero Map of $v(s)\delta FER(s)$	44
Figure 4.5: Open Loop $A0A$, q and Θ (Incremental Values)	45
Figure 4.6: Open Loop V and H (Incremental Values)	46
Figure 4.7: General Pitch-Axis Stability Control Loop	47
Figure 4.8: Baseline Pitch SAS Control System	48
Figure 4.9: Elevator Input and Pitch Rate Response with Dynamic Inversion Controller	48

Figure 4.10: Baseline Control with Adaptive Regulator	49
Figure 4.11: Elevator Input and Pitch Rate with Adaptive Regulator	49
Figure 4.12: Elevator Input and Pitch Rate (Rigid body model)	50
Figure 4.13: Elevator Input and Pitch Rate (Flexible body model)	50
Figure 4.14: δ_e to q loop with adaptive controller for the flexible Model	51
Figure 4.15: General Speed-Hold Control Law	52
Figure 4.16: Mach-Hold W/ Command Augmentation Proposed	53
Figure 4.17: <i>FER</i> to v Loop with Adaptive Controller for the Flexible Model	53
Figure 4.18: Combined <i>FER</i> to v and δ_e to q Adaptive Controller Loops on the Flexible Model	55
Figure 4.19: Elevator and FER Input	55
Figure 4.20: Outputs TAS and Altitude	55
Figure 4.21: AoA, Pitch Rate and Pitch Angle	56
Figure 4.22: Modal Coordinate and Velocity	56
Figure 4.23: Mach-Hold and Command Control System	57
Figure 4.24: Pitch-Axis Stability Augmentation and Mach-Hold and Command Augmentation Control System	57
Figure 4.25: TAS, Delta Speed Command and FER Input	58
Figure 4.26: Control System on the Nonlinear Model	59
Figure 4.27: Elevator and FER input	59
Figure 4.28: AoA, Pitch Rate and Pitch Angle	60
Figure 4.29: TAS and Altitude	60
Figure 4.30: Modal Velocity and Coordinate	60
Figure 4.31: Zero Location before and After Sensor Blending	62
Figure 4.32: Elevator Input and Pitch Rate Response (Unblended System)	62

Figure 4.33: Elevator Input and Pitch Rate Response (blended System)	63
Figure 5.1: Multivariable Zeros	66
Figure 5.2: Zeros of $qs\delta es$ vs Multivariable Zeros Overlay	68
Figure 5.3: Zeros of $vs\delta FERS$ vs Multivariable Zeros Overlay.....	68
Figure 5.4: System in Normal Form	71
Figure 5.5: Zeros of $qs\delta es$ vs Multivariable Transmission Zeros Overlay.....	73
Figure 5.6: Zeros of $vs\delta FERS$ vs Multivariable Transmission Zeros Overlay	73
Figure 5.7: Multivariable System and Control System.....	75
Figure 5.8: System Inputs	76
Figure 5.9: TAS and Altitude.....	76
Figure 5.10: Modal Coordinate and Velocity	76
Figure 5.11: System Output	76
Figure 5.12: Input Command Speed and Elevator Deflection for Test Cases	77
Figure 5.13: Speed, Speed tracking error and pitch rate (Red - Baseline, Blue - Case 2)	78
Figure 5.14: Speed, Speed tracking error and pitch rate (Red - Baseline, Blue - Case 3)	78
Figure 5.15: Speed, Speed tracking error and pitch rate (Red - Baseline, Blue - Case 1)	79
Figure 5.16: Speed, Speed tracking error and pitch rate (Red – SISO System, Blue – MIMO Case 1)	80
Figure 6.1: Directionally Unstable for $AoA < 2$ deg (Low Speed) (Mutzman, et al 2011).....	83
Figure 6.2: Laterally Unstable for $AoA < 6$ Deg (Low Speed) (Mutzman, et al 2011)	84
Figure 6.3: Laterally Unstable for $AoA < 9$ Deg (low Speed) (Mutzman, et al 2011)	84

LIST OF TABLES

Table 3.1: Actuator Model (Bolender, 2009; Korad, 2010)	28
Table 3.2: States for Hypersonic Vehicle Model.....	30
Table 3.3: Controls for Hypersonic Vehicle Model.....	31
Table 3.4: Vehicle Nominal Parameter Values (Korad, 2010).....	32
Table 3.5: Vehicle Dimensions (Bolender, et al 2007).....	33
Table 3.6: State Variables	35
Table 3.7: Controls Variables	36
Table 4.1: Optimized Values for Trim Condition.....	39
Table 4.2: Poles location, ω_n and ζ for longitudinal and structural modes	42
Table 4.3: Zeros for transfer function $q(s)\delta e(s)$ and $v(s)\delta FER(s)$	44
Table 5.1: SISO Zeros vs Multivariable Zeros	67
Table 5.2: Multivariable Zeros Set VS Transmission Zeros Set	72
Table 5.3: SISO vs Transmission Zeros Comparison.....	74
Table 5.4: Coupling Weightings	77

SYMBOLS

The following is a list of variables with their respective units, which are used throughout the report.

h	Altitude	(ft)
α	Angle of Attack	(deg)
\bar{q}	Dynamic Pressure	(lbs/ft ²)
δ_e	Elevator Deflection	(deg)
h_i	Engine Inlet Height	(ft)
η_1	First Flexible Mode	(rad)
$\dot{\eta}_1$	First Flexible Mode Rate	(rad/s)
N_i	i th Generalized Modal Force	(rad/s ²)
Φ_i	i th mode shape	(-)
Θ	Pitch Angle	(deg)
q	Pitch Rate	(deg/sec)
p_1	Pressure at the engine inlet, behind the shock	(lbs/ft ²)
η_2	Second Flexible Mode	(rad)
$\dot{\eta}_2$	Second Flexible Mode Rate	(rad/s)
β	Shock angle	(deg)
V	Speed	(kft/sec)
M_1	Speed of flow in the engine inlet, behind the shock	(Mach)
T_e	Temperature at the engine exit	(°R)
T_1	Temperature at the engine inlet, behind the shock	(°R)
η_3	Third Flexible Mode	(rad)
$\dot{\eta}_3$	Third Flexible Mode Rate	(rad/s)
A_d	Diffuser Area Ratio	
A_n	Exit nozzle area ratio	

ABBREVIATIONS

<i>AFRL</i>	Air Force Research Lab	
<i>AoA</i>	Angle of Attack	(deg)
<i>APR</i>	Almost Positive Real	
<i>ASD</i>	Almost Strictly Dissipative	
<i>ASPR</i>	Almost Strictly Positive Real	
<i>CG</i>	Center of Gravity	
<i>CAS</i>	Command Augmentation System	
<i>CFD</i>	Computational Fluid Dynamics	
<i>DOF</i>	Degree of Freedom	
<i>FM</i>	Flexible Mode	
<i>FPA</i>	Flight Path Angle	
<i>FER</i>	Fuel Equivalence Ratio	
<i>HSV</i>	Hypersonic Vehicle	
<i>MatLab</i>	Matrix Laboratory	
<i>MRAC</i>	Model Reference Adaptive Control	
<i>MIMO</i>	Multiple Input Multiple Output	
<i>PDE</i>	Partial Differential Equation	
<i>PR</i>	Positive Real	
<i>RHP</i>	Right Hand Plane	
<i>SEC</i>	Seconds	
<i>SISO</i>	Single Input Single Output	
<i>SAS</i>	Stability Augmentation System	
<i>SD</i>	Strictly Dissipative	
<i>WPAB</i>	Wright-Patterson Air Force Base	

ABSTRACT

Aditya, Ron MSAE, Embry-Riddle Aeronautical University, December 2015. Direct Adaptive Control for Stability and Command Augmentation System of an Air-breathing Hypersonic Vehicle

In this paper we explore a Direct Adaptive Control scheme for stabilizing a non-linear, physics based model of the longitudinal dynamics for an air breathing hypersonic vehicle. The model, derived from first principles, captures the complex interactions between the propulsion system, aerodynamics, and structural dynamics. The linearized aircraft dynamics show unstable and non-minimum phase behavior. It also shows a strong short period coupling with the fuselage-bending mode. The value added by direct adaptive control and the theoretical requirements for stable convergent operation is displayed. One of the main benefits of the Direct Adaptive Control is that it can be implemented knowing very little detail about the plant. The implementation uses only measured output feedback to accomplish the adaptation. A stability analysis is conducted on the linearized plant to understand the complex aero-propulsion and structural interactions. The multivariable system possesses certain characteristics beneficial to the adaptive control scheme; we discuss these advantages and ideas for future work.

Page Intentionally Left Blank

1. INTRODUCTION

1.1 Hypersonic Flight Background

Air-breathing hypersonic aircraft are seen as a possible solution to making access to space routine and affordable. The historic 2004 scramjet-powered Mach 7 and 10 flights of the X-43A (Volland, et al 2005; McClinton 2006; Rausch, et al 1997) have revived hypersonic research. In the 1990's, the Air Force Research Laboratory (AFRL) began the HyTECH program for hypersonic propulsion. Pratt and Whitney received a contract from the AFRL to develop a hydrocarbon-fueled scramjet engine, which led to the development of the SJX61 engine. The SJX61 engine was originally meant for the NASA X-43C, which was eventually cancelled. The engine was applied to the AFRL's Scramjet Engine Demonstrator program in late 2003 (Letsinger, 2012). The scramjet flight test vehicle was designated X-51 in September 2005.

In flight demonstrations, the X-51 is carried to an altitude of 50,000 feet by a B-52 and released over the Pacific Ocean (Air Force Times, 2009). The X-51 is initially propelled by an MGM-140 ATACMS solid rocket booster to approximately Mach 4.5. The booster is then jettisoned and the vehicle's Pratt and Whitney Rocketdyne SYJ61 scramjet, using JP-7 fuel, accelerates it to a top flight speed near Mach 6 – 8 (Villanueva, 2007; Wright-Patterson Air Force Base News, 2010). A layout of the mission profile is shown in Figure 1.1.

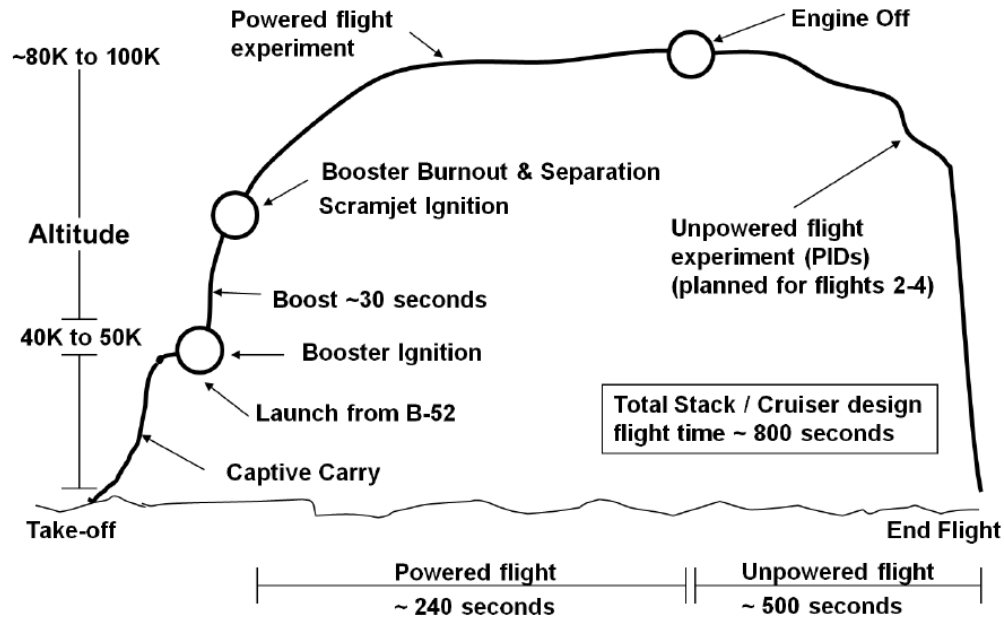


Figure 1.1: X-51 Mission Profile (Mutzman, et al 2011)

During this 8 year long program the Air Force Research Lab, Wright-Patterson Air Force Base, developed a modeling environment that control engineers could use early in the design process to help understand the physical manifestation of the complex interactions between the aerothermodynamics, propulsion system, control system, and structural dynamics that occur for a given configuration (Bolender, 2009).

The team at AFRL maintained the philosophy that the aerodynamic forces and moments are not stored in look-up tables, but instead calculated at each time step of the simulation given the actuation of the controls and the current state of the vehicle. This approach takes the simulation much closer to the real dynamics than a mathematical model.

The idea of this modeling effort from the start has been to incrementally add complexity to the model. The initial model was based on the assumption of quasi-steady airflow over the vehicle, which allowed oblique shock theory and Prandtl-Meyer flow to

determine the pressure distribution on the vehicle. This approach was replaced by linear piston theory in order to capture the unsteady components of the flow field. The original model was based on the assumption of inviscid flow; an analytical skin friction model using Eckert's reference temperature method is incorporated into the model to give more realistic drag estimates (Bolender, et al 2006).

Changes were made to the Aeroelastic model to improve the estimation of the mode shapes and frequencies of the structural dynamics. By utilizing the Assumed Modes Method, it was possible to calculate any desired number of frequencies and mode shapes (Doman, et al 2006). In the following section, we will review the history and evolution of adaptive controls and describe the problem and the proposed solution.

1.2 Adaptive Controls Literature Survey

Research in adaptive control has a long history of intense activities that involved debate about the precise definition of adaptive control, examples of instabilities, stability and robustness proofs, and applications (Ioannou, et al 2012).

Starting in the early 1950s, the design of autopilots for high performance aircraft motivated intense research activity in adaptive control (Ioannou, et al 2012). High performance aircraft have a highly non-linear flight envelope that cannot be handled by constant gain feedback control. Gain scheduling or other linear control approaches demand linearization at hundreds and thousands of operating points. This created a demand for a sophisticated controller, such as an adaptive controller, that could learn and accommodate changes in the flight dynamics (Ioannou, et al 2012). MRAC was suggested by Whitaker

in (Osburn, et al 1961; Whitaker, et al 1958) to solve the autopilot control problem, which used sensitivity method and MIT rule to design the adaptive law of the various proposed adaptive control scheme.

The field of adaptive control over time has advanced to be one of the richest in terms of design techniques, algorithms, analytical tools, and modifications. Books such as Stable Adaptive Systems by Narendra and Annaswamy (Narendra, et al 2012), Adaptive Control by Åström† and Wittenmark (Åström†, et al 1989), Adaptive Filtering, Prediction and Control by Goodwin and Sin (Goodwin, et al 1984) , Robust Adaptive Control by Ioannou and Sun (Ioannou, 2012) and published research monographs (Fuentes, et al 2000; Balas, et al 2016; Balas, 2012; Wen, 1989; Tsytkin, 1971; Harris, et al 1981; Unbehauen, 1980; Chalam, 1987; Egardt, 1979) already exist on the topic of adaptive control.

The terms “adaptive control” and “adaptive systems” have been used as early as 1950 (Aseltine, et al 1985; Caldwell, 1950). The design of autopilots for high-performance aircraft was one of the primary motivations for active research on adaptive control in the early 1950s (Ioannou, 2012). Aircraft operate over a wide range of speeds and altitudes, and their dynamics are non-linear and conceptually time varying (Ioannou, 2012). For a given operating point, specified by the aircraft speed (Mach number) and altitude, the complex aircraft dynamics can be approximated by a linear model of the form:

$$\begin{cases} \dot{x} = Ax + Bu, & x(0) = x_0 \\ y = Cx + Du \end{cases}$$

Where $x \in \mathbf{R}^n$ is the state of the model, $u \in \mathbf{R}^r$ the plant input, if $y \in \mathbf{R}^p$ the plant model output. The matrices $A \in \mathbf{R}^{n \times n}$, $B \in \mathbf{R}^{n \times r}$, $C \in \mathbf{R}^{p \times n}$ and $D \in \mathbf{R}^{p \times r}$ could be

constant or time varying. For an operating point i , the linear aircraft model takes the following form:

$$\begin{cases} \dot{x} = A_i x + B_i u, & x(0) = x_0 \\ y = C_i x + D_i u \end{cases}$$

Where A_i, B_i, C_i and D_i are functions of the operating point i . As the aircraft goes through different conditions, the operating point changes leading to different values of A_i, B_i, C_i and D_i . $y(t)$ the output response carries information about the state x as well as the parameters, thus a sophisticated feedback controller should be able to learn about parameter changes by processing $y(t)$ and using the appropriate gains to compensate them. This ideology led to the feedback control structure upon which adaptive control is based (Narendra, 2005). The controller structure consists of a feedback loop and a controller with adjustable gains as shown in Figure 1.2 (Ioannou, et al 2012). The way of adjusting the controller gains in response to variation in the plant and disturbance dynamics differentiates one scheme from another.

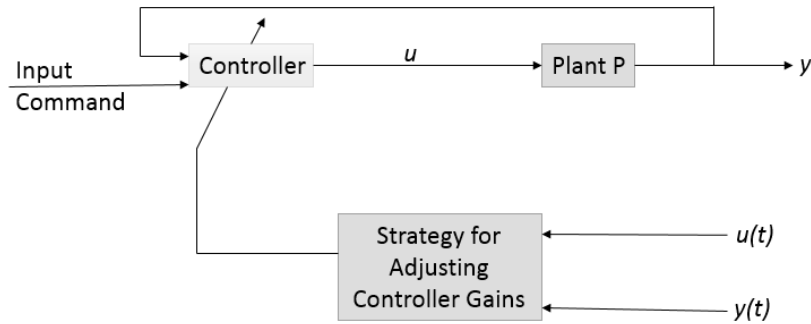


Figure 1.2: General Adaptive Controller Structure (Ioannou, et al 2012)

This control law is formulated by merging an on-line parameter estimator, providing estimates of unknown parameters at each instance, with the control law that is

driven from the known parameter case. Adaptive controls bifurcate into two categories. In indirect adaptive control, the plant parameters are estimated on-line and used to calculate the controller parameters. This approach is also known as explicit adaptive control (Ioannou, et al 2012).

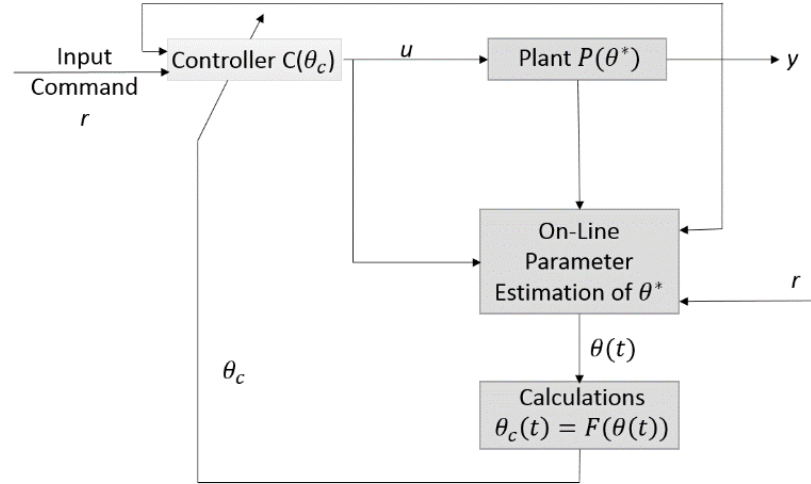


Figure 1.3: Principle Structure of Indirect Adaptive Control (Ioannou, et al 2012)

In indirect adaptive control, the plant model $P(\theta^*)$ is parameterized with respect to some unknown parameter vector θ^* with θ^* representing unknown coefficients of the transfer function. So, an on-line parameter estimator builds an estimate $\theta(t)$ of θ^* at each time step by processing the input u to the system and output y from the system. The parameter estimates $\theta(t)$ specifies an estimated plant model characterized by $\hat{P}(\theta(t))$, which is used to calculate the controlled parameters vector $\theta_c(t)$ by solving the algebraic equation $\theta_c(t) = F(\theta(t))$ at each time t .

The second approach is called direct adaptive control. Ioannou and Sun define this as where “the plant model is parameterized in terms of the controller parameters that are

estimated directly without intermediate calculations involving plant parameter estimates” (Ioannou, et al 2012), shown in Figure 1.4.

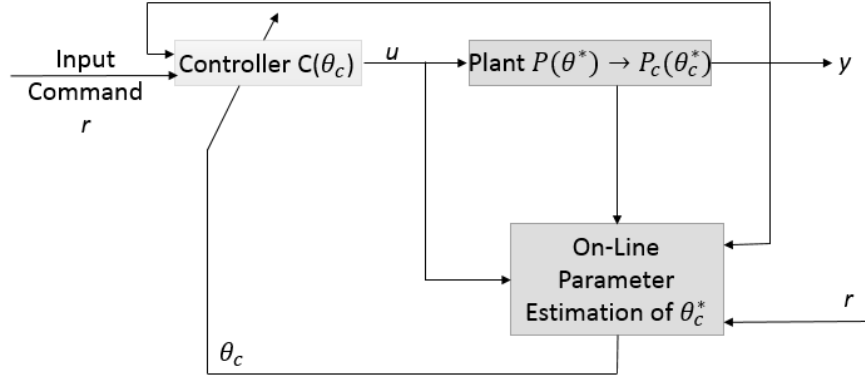


Figure 1.4: Design Principle of Direct Adaptive Control (Ioannou, et al 2012)

In contrast to this Narendra and Annaswamy define “direct adaptive control as where no effort is made to identify the plant parameter but the control parameters are directly adjusted to improve a performance index” (Narendra, et al 2005), shown in Figure 1.5 where M is the model reference plant, P is the plant and C is the controller.

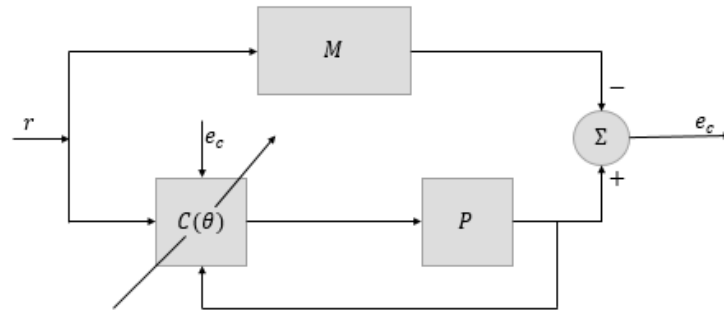


Figure 1.5: Design Principle of MR Direct Adaptive Control (Narendra, et al 2012)

The first step in the stability approach to adaptive system design is the choice of the adaptive law for adjusting the control parameters to assure stability. Narendra and

Annaswamy define this class of direct adaptive schemes as error models (Narendra, et al 2005). For this scheme let θ^* be a constant unknown vector such that the output of the adaptive system follows the output of the reference model exactly when $\theta(t) \equiv \theta^*$. The state error vector $e(t)$ and the parameter error vector $\phi(t)$ are defined as:

$$e(t) \triangleq x(t) - x^*(t), \quad \phi(t) \triangleq \theta(t) - \theta^*$$

Where $x^*(t)$ is the desired trajectory. The goal is for $e(t)$ to tend to zero as $t \rightarrow \infty$, in the absence of external disturbances. In many cases, it is also desirable to assure that $\lim_{t \rightarrow \infty} \phi(t) = 0$. This approach was first suggested by Narendra (Narendra, et al 1971) in 1971. This can also be represented in terms of the error vector. Focusing attention directly on the error/error vector, rather than on the actual response of the plant or reference model enables the designer to concentrate on the essential features of the problem (Narendra, et al 2005).

Based on this philosophy Wen and Balas (Wen, et al 1989) developed Narendra's direct adaptive scheme a class of error model adaptive control law in infinite dimensional space in 1989 (Wen, et al 1989), shown in Figure 1.6. This scheme in particular was one of the very first that generalized the finite-dimensional control law to the infinite-dimensional Hilbert Space. Here a finite-dimensional adaptive controller was modified and Lagrange stability was proved for closed-loop systems close to being positive real. This was a major advancement from Wen's previous work in (Wen, 1985).

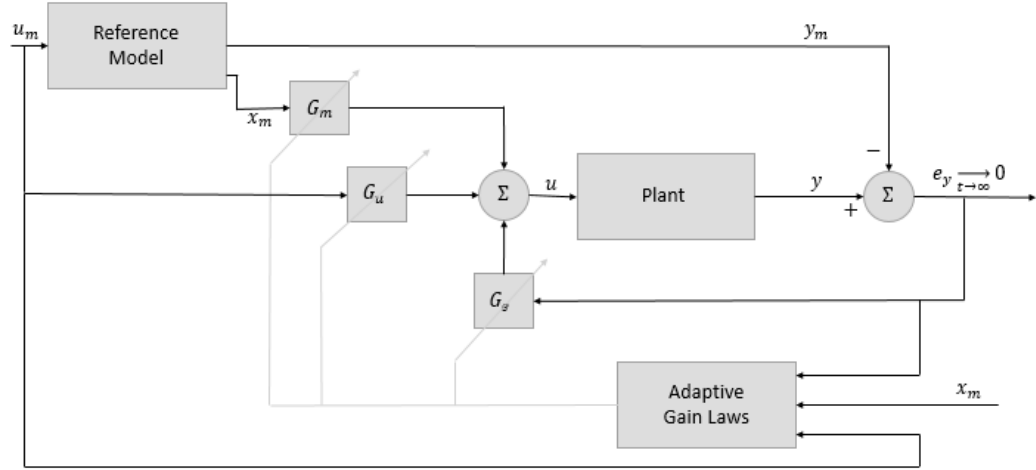


Figure 1.6: Error Model Class MRAC Scheme (Wen, et al 1989)

In the late 1990s, a relatively large amount of attention was devoted to stochastic disturbances in the system and references were scarce on deterministic noise compensation. Fuentes and Balas (Fuentes, et al 2000) generated a new scheme in 2000 for the error model class of adaptive control. They illustrated a technique, complementing the previous MRAC work and guaranteed asymptotically stable tracking in the presence of external disturbances, shown in Figure 1.7.

This scheme has served as a foundation for future work. Over the years the control law has been modified and reformulated. In the mid and late 2000s the majority of the attention was devoted to formulating techniques in order to meet the stability theorem requirements. The fundamental hypothesis for direct adaptive control is developed in (Balas, et al 2004) for both ASPR and APR systems. Efforts have also been made and MRAC now has been shown to handle unknown delays and persistent disturbances (Balas, et al 2009).

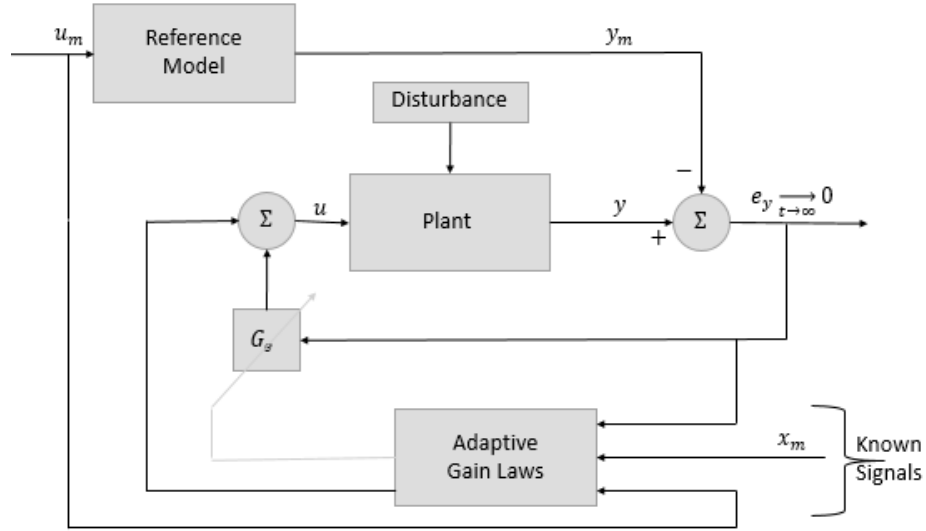


Figure 1.7: Error Model Class MRAC Scheme with Persistent Disturbance Rejection (Fuentes, et al 2000)

These efforts have broadened the class of systems MRAC can be implemented on, which has allowed researchers to conduct experiments using this scheme. Since 2010, focus has been put on formulating stronger and more sophisticated stability proofs along with testing the control law on various linear, nonlinear, linear time invariant and time varying systems (Balas, et al 2012; Balas, et al 2012; Schlipf 2013).

Stability proofs have been formulated for periodic linear time varying systems (Li, et al 2014). Sophisticated techniques like sensor blending and use of zero filters to mitigate non-minimum phase have already been published (Balas, et al 2012; Hartman, 2012).

A complete stability analysis in infinite-dimensional space, ease of implementation and need of very little information about the plant make this control law a viable scheme for systems with high order and a large number of parameters.

1.3 Problem Description

A number of recent flight test programs have demonstrated the feasibility of airbreathing hypersonic flight (Volland, et al 2005; McClinton 2006). The flight test vehicles flown to date were relatively small in scale, stiff, and some were statically stable. Large scale scramjet powered aircraft designed for long range cruise or access to space are generally unstable and mechanically flexible which leads to significant control challenges.

The coupling between the aerodynamics, propulsion system, structure, controls, and thermal system presents a complex modeling and control problem (Bolender, 2009; Bolender, et al 2007; Bolender, et al 2007; Bolender, et al 2006; Doman, et al 2006; Oppenheimer, et al 2007). CFD models with coupled aerodynamic and structural grids provide the most accurate tools for analysis of such systems; however, they are not well suited for control design. Even with the use of such sophisticated computational tools, there is a considerable amount of uncertainty in even relatively stiff entry-vehicle models and major differences between predicted and observed behavior have been found in practice (Cobleigh, 1998).

One approach to control design and analysis is to make use of control-oriented models that capture the salient aerothermoservoelastic features of large-scale hypersonic vehicles (Bolender, 2009; Bolender, et al 2007; Oppenheimer, et al 2007). This allows one to quickly explore control strategies, identify fundamental control challenges, and to quickly assess performance before moving toward more costly and time-consuming high fidelity simulation models for testing.

Hypersonic vehicles due to a long fore body and aft engine tend to have an aft CG creating nose-up pitching moment (instability). The long structure and issues of heating at

the forebody restricts placement of any control surfaces like canards in the forebody; an aft control surface gives the system a non-minimum phase characteristic.

This presents control challenges and performance limitations for any control method. The high levels of uncertainty present in even the highest fidelity models motivate the exploration of adaptive control methods for use with large-scale scramjet powered hypersonic aircraft. Elements of the control-oriented models described in (Bolender, 2009; Bolender, et al 2007; Oppenheimer, et al 2007) are used in the present work to design a stability and command augmentation system using a direct adaptive control scheme that is capable of adapting to nonlinearities.

The X-51 being a successful scramjet engine demonstrator, we use the nonlinear simulation as a platform to evaluate the control scheme for providing artificial longitudinal stability.

The usual mission profile for the X-51 hypersonic demonstrator consists of a drop from the B-52 at 50,000 feet after which a rocket booster climbs and accelerates the vehicle to Mach 4.5. At this point the booster separates, the scramjet engine is ignited and the vehicle cruises at this altitude with slow incremental increases in speed (need for speed command augmentation) until it runs out of fuel and crashes in the ocean.

In this work we take the problem of instability and requirement for tracking a speed command and use an adaptive control scheme, obscure in terms of application until very recently, to compensate for longitudinal instability by providing artificial longitudinal stability and track a speed command.

We achieve longitudinal stability by designing a pitch-axis stability augmentation and enable accurate speed command tracking by designing a speed command and hold augmentation using the direct adaptive control scheme mentioned previously in section 1.2.

In Chapter 2, we examine the direct adaptive control scheme and the stability theory upon which this thesis relies. We look at the requirements a system must meet in order to satisfy the nonlinear stability theorem. The linearized plant being non-minimum phase we discuss ways of mitigating this. In Chapter 3 we briefly discuss the hypersonic model derived by the AFRL team (Bolender, 2009; Bolender, et al 2007; Bolender, et al 2007; Bolender, et al 2006; Doman, et al 2006; Oppenheimer, et al 2007) and also look at the simulation model coded using Matlab and Simulink.

In Chapter 4, we discuss the conventional ideas behind the design of a pitch-axis stability augmentation system and speed command and hold augmentation system. We discuss the two proposed control laws and review the results from the linearized and nonlinear simulation. In order to mitigate non-minimum phase, we conduct sensor blending on the linearized plant in order to meet the conditions of the stability theorem.

In Chapter 5, we design the stability and command control law through a multivariable approach. We briefly discuss multivariable systems and the two broad categories. Next we look at the stability requirements for the control scheme in case of multivariable systems and discuss the definition of transmission zeros. We then look at ways of computing these transmission zeros and implement the direct adaptive scheme and also compare performance characteristics for different coupling weightings and with the

SISO case. In Chapter 6, we discuss some conclusions gathered from the observations and results in Chapter 4 and 5 and also discuss areas of interest for future work.

2. DIRECT ADAPTIVE CONTROL SCHEME

In this section, we review the results of (Balas, et al 2014; Balas, et al 2003) for the direct adaptive scheme mentioned in section 1.2. Let $X \equiv \mathbf{R}^N$ with the usual inner product (x, y) and corresponding norm $\|x\| \equiv \sqrt{(x, x)}$. Consider the linear finite-dimensional plant:

$$\begin{cases} \dot{x} &= Ax + Bu \\ y &= Cx, x^0 \equiv x(0) \in \mathbb{R}^N \end{cases} \quad (1)$$

Where $A: \mathbf{R}^N \rightarrow \mathbf{R}^N$, $B: \mathbf{R}^M \rightarrow \mathbf{R}^N$, and $C: \mathbf{R}^N \rightarrow \mathbf{R}^M$ are real valued matrix operators. We define (1) to be globally exponentially stable if $\text{Re}(\lambda_i(A)) < 0$ for eigenvalues

$$\lambda_i, i = 1, \dots, N \quad (2)$$

This system is said to be output feedback stabilizable if there exists $G^*: \mathbf{R}^M \rightarrow \mathbf{R}^M$ such that the operator $(A + BG^*C): \mathbf{R}^N \rightarrow \mathbf{R}^N$ is exponentially stable. We say the triplet (A, B, C) is strictly dissipative (SD) if (A, B) is controllable, and there exist symmetric positive definite matrix operators $P, Q \in \mathbf{R}^{N \times N}$ such that:

$$\begin{cases} A^T P + PA &\leq -Q \\ PB &= C^T \end{cases} \quad (3)$$

These equations are called the Kalman-Yacubovic (K-Y) equations. Almost strict dissipativity is defined here as $\exists G_* \ni (A + BG_*C, B, C)$ is SD. For the non-adaptive model-tracking control design, we are given a plant model

$$\begin{cases} \dot{x}_p &= A_p x_p + B_p u_p \\ y_p &= C_p x_p; x_p^0 \equiv x_p(0) \in \mathbf{R}^{N_p}, \end{cases} \quad (4)$$

Having $u_p, y_p \in \mathbf{R}^M$ with the equations in (1) output feedback is stabilizable by gain G_e^* .

The above system is required to track the reference trajectory output of the following stable reference model:

$$\begin{cases} \dot{x}_m &= A_m x_m + B_m u_m \\ y_p &= C_p x_p; x_m^0 \equiv x_m(0) \in \mathbf{R}^{N_p} \\ N_m &\leq N_p, y_m \in \mathbf{R}^M \end{cases} \quad (5)$$

With excitation:

$$\begin{cases} \dot{z}_m &= F_m z_m \\ u_m &= \theta_m q_m; q_m^0 \equiv q_m(0) \in \mathbf{R}^{N_m} \end{cases} \quad (6)$$

We assume that all the trajectories of (6) are bounded, and that (5) is exponentially stable. An ideal trajectory is assumed such that the ideal output matches that of the reference model:

$$\begin{cases} \dot{x}_* &= A_p x_* + B_p u_* \\ y_* &= C_p x_* = y_m \end{cases} \quad (7)$$

If there exists a transformation, (8), which satisfies the matching conditions given by (9), we say that (5 – 7) are totally consistent:

$$\begin{bmatrix} x_* \\ u_* \end{bmatrix} = \begin{bmatrix} S_{11}^* & S_{12}^* \\ S_{21}^* & S_{22}^* \end{bmatrix} \begin{bmatrix} x_m \\ z_m \end{bmatrix} \quad (8)$$

$$\begin{aligned} A_p S_{11}^* + B_p S_{21}^* &= S_{11}^* A_m \\ (A_p S_{21}^* + B_p S_{22}^*) C_q &= S_{11}^* B_m C_q + S_{12}^* C_q A_q \\ C_m S_{11}^* &= C_m \\ C_p S_{12}^* &= 0. \end{aligned} \quad (9)$$

Define $e_y \equiv y_p - y_m$ as the output tracking error, $e_* \equiv x_p - x_*$ as the state tracking error and the control input for the system in (4) as:

$$u_p = S_{21}^* x_m + S_{22}^* u_m + G_e^* e_y. \quad (10)$$

The closed loop can be shown to produce asymptotic output tracking, $e_y \rightarrow 0$ as $t \rightarrow \infty$, when the complete knowledge of the plant is assumed and the matching conditions are solved.

However, the following fundamental direct adaptive control result is valid without solving the matching conditions in equations (8) and (9):

Theorem 1: If (A_p, B_p, C_p) is ASD, and (5), (6), and (7) are totally consistent, then the adaptive gain laws,

$$\begin{aligned}\dot{S}_{21} &= -e_y x_m^T H_1 \\ \dot{S}_{22} &= -e_y u_m^T H_2 \\ \dot{G}_e &= -e_y e_y^T H_3\end{aligned} \quad H_i \text{ positive definite} \quad (11)$$

along with the control law,

$u_p = S_{21}x_m + S_{22}u_m + G_e e_y$, produce asymptotic output tracking ($\lim_{t \rightarrow \infty} e_y = 0$) with uniformly bounded adaptive gains (S_{21}, S_{22}, G_e) .

Stability theorem proof: It is evident that

$$\begin{cases} \dot{e}_* &= A_p e_* + B_p \Delta u \\ e_y &= C_p e_* \\ \Delta u &= u_p - u_* = G_e^* e_y + w \\ w &\equiv \Delta G z \end{cases} \quad (12)$$

Where the data error $z \equiv [x_m^T u_m^T e_y^T]^*$ and $\Delta G \equiv G - G_*$ with $G \equiv [S_{21} S_{22} G_e]$ and $G_* \equiv [S_{21}^* S_{22}^* G_e^*]$. Therefore

$$\begin{cases} \dot{e}_* &= A_c e_* + B_p w \\ e_y &= C_p e_* \\ A_c &\equiv A_p + B_p G_e^* C_p \end{cases} \quad (13)$$

$$\begin{aligned} \text{Let } V_1 &\equiv \frac{1}{2} e_*^T P_c e_*. \text{ Then } \dot{V}_1 \equiv \frac{1}{2} (\dot{e}_*^T P_c e_* + e_*^T P_c \dot{e}_*) = \frac{1}{2} e_*^T (A_c^T P_c + P_c A_c) e_* + e_*^T P_c B_p w = \\ &\leq -\frac{1}{2} e_*^T Q_c e_* + e_y^T w \end{aligned} \quad (14)$$

using (10) since (A_c, B_p, C_p) is SPR. Now let $V_2 \equiv \frac{1}{2} \text{tr}(\Delta G H^{-1} \Delta G^T)$.

$$\begin{aligned} \Rightarrow \dot{V}_2 &= \text{tr}(\Delta G H^{-1} \Delta \dot{G}^T) \\ &= \text{tr}(\Delta G H^{-1} (-e_y z^T H)^T) = -\text{tr}(\Delta G z e_y^T) \\ &= -e_y^T w. \end{aligned} \tag{15}$$

Because

$$\Delta \dot{G} = -e_y z^T H \tag{16}$$

from (11) with positive definite $H \equiv \text{diag}(H_1, H_2, H_3)$.

Taking the Lyapunov function $V \equiv V_1 + V_2$.

$$\begin{aligned} \Rightarrow \dot{V} &= -\frac{1}{2} e_*^T Q_c e_* + e_y^T w + (-e_y^T w) \\ &= -\frac{1}{2} e_*^T Q_c e_* \leq 0 \end{aligned} \tag{17}$$

Lyapunov theory guarantees the stability of the zero equilibrium point of (13) and (16), and we have e_* and ΔG bounded. Since x_m , u_m and $e_y = C_p e_*$ are bounded, this implies that z is bounded. The second derivative of the Lyapunov function is

$$\ddot{V} \leq -2e_*^T Q_c \dot{e}_* = -2e_*^T Q_c (A_c e_* + B_p \Delta G z) \tag{18}$$

$$\leq -2 \cdot \|e_*\| \cdot \|Q_c\| \cdot (\|A_c\| \|e_*\| + \|B_p\| \cdot \|\Delta G\| \cdot \|z\|) \leq M, \tag{19}$$

for some $M > 0$. Equation (18) is bounded because each term in (19) is bounded in the appropriate norm. Invoking the mean value theorem, we have $|\dot{V}(t_1) - \dot{V}(t_2)| \leq M|t_1 - t_2| \forall t_1, t_2 \in \mathbb{R}$. Hence $\dot{V}(t)$ is uniformly continuous, so by Barbalat's lemma (Popov, et al 1973) ($\lim_{t \rightarrow \infty} \dot{V}(t) = 0$). Hence, we have ($\lim_{t \rightarrow \infty} e_* = 0$) because Q_c is positive definite in (17) the output tracking error has the property of asymptotic stability with ($\lim_{t \rightarrow \infty} e_y = 0$) and ($\lim_{t \rightarrow \infty} C_p e_* = 0$). Furthermore, since ΔG is uniformly bounded, we have

that the gains, S_{21} , S_{22} and G_e are uniformly bounded. End of proof. In the following section, we show how a persistent disturbance can be rejected.

Persistent disturbance rejection: Consider the linear finite-dimensional plant with persistent disturbance:

$$\begin{cases} \dot{x} = Ax + Bu + \Gamma u_D \\ y = Cx \end{cases} \quad (20)$$

where x is the plant state, $u, y \in \mathbf{R}^M$ are the control input and plant output, respectively, and u_D is a persistent disturbance input (Balas, et al 2013). We will follow the development given in (Balas, et al 2014).

Definition: A disturbance vector $u_D \in \mathbf{R}^q$ is said to be persistent if it satisfies the disturbance generator equations:

$$u_D = \theta z_D$$

$$\dot{z}_D = F z_D$$

Or

$$u_D = \theta z_D$$

$$z_D = L \phi_D$$

where F is a marginally stable matrix and ϕ_D is a vector of known functions forming a basis for all such possible disturbances. This is known as “a disturbance with known wave form but unknown amplitude”. The adaptive controller must eliminate or mitigate all linear combinations of the known disturbance basis functions.

The objective of control in this paper is to cause the output y of the plant to asymptotically track the model output y_m of a linear finite-dimensional reference model given by:

$$\begin{cases} \dot{x}_m &= A_m x_m + B_m u_m, \\ y_m &= C_m x_m, x_m(0) = x_0^m, \end{cases}$$

Where the reference model state x_m is an N_m - dimensional vector with reference model output y . In general, the plant and reference models need not have the same dimension. The excitation of the reference model is accomplished via u_m which is generated by

$$\begin{aligned} \dot{u}_m &= F_m u_m, \\ u_m(0) &= u_0^m. \end{aligned}$$

The reference model parameters (A_m, B_m, C_m, F_m) will be assumed known. The meaning of asymptotic tracking is as follows.

We define the output error vector as

$$e_y \equiv y - y_m \xrightarrow{t \rightarrow \infty} 0,$$

The control objective will be accomplished by a direct adaptive control law in the form of

$$u = G_m x_m + G_u u_m + G_e e_y + G_D \phi_D$$

The direct adaptive controller will have adaptive gains given by (Balas, et al 2014)

$$\begin{aligned} \dot{G}_u &= -e_y u_m^* \gamma_u, \quad \gamma_u > 0 \\ \dot{G}_m &= -e_y x_m^* \gamma_m, \quad \gamma_m > 0 \\ \dot{G}_e &= -e_y e_y^* \gamma_e, \quad \gamma_e > 0 \\ \dot{G}_D &= -e_y \phi_D^* \gamma_D, \quad \gamma_D > 0 \end{aligned}$$

2.1 System Requirements

An aircraft model, characterized by its aerodynamic behavior, propulsion system performance, weight, center of gravity (x_{cg}) position, airspeed, altitude, flight path angle and structural modes is subject to a wide range of parameter variations. These characteristics change its dynamics and for this reason a dynamic mode that is stable and adequately damped in one flight condition may become unstable or at least inadequately damped in another flight condition creating a need for self-adjusting controllers. For the given problem, the system also exhibits an unstable behavior. Thus in order to solve this issue we design a pitch-axis stability augmentation system using a direct adaptive control scheme.

Implementation of this control scheme requires a very little knowledge of the plant. To ensure error convergence to zero and bounded gains the open loop plant must have (Balas, et al 2014):

- CB positive definite and symmetric, sign definite for scalar CB .
- Absence of RHP transmission zeros.

These are sufficient conditions for ASD; although even if not satisfied, the direct adaptive control law may still work. However, by meeting these requirements one can be assured of bounded adaptive gains and error convergence to zero. In practice, aircraft models are linearized at various points of the flight envelope and a linear controller is tuned for every linearized section of the flight envelope. In the case of hypersonic air-breathing vehicles this becomes a very difficult task as breaking down the flight envelope for linearization would result in numerous models varying in mass, dimensions, number of

control surfaces, etc. A nonlinear direct adaptive controller that ensures adaptability to parametric changes along with providing artificial stability and global asymptotic stability seems essential.

All tail-controlled aircraft are non-minimum phase systems. Thus in order to assure adaptation, ways of mitigating non-minimum phase behavior have been developed (Balas, 2012; Hartman, 2012) and are discussed in the following section.

2.2 Non-Minimum Phase Mitigation

Sensor blending is a method of alleviating the non-minimum phase behavior of a system. The idea is to manipulate the output feedback in order to present the adaptive controller with a system that is minimum phase (Balas, 2012; Hartman, 2012). There are a few ways this could be achieved, namely zero-relocation and minimum phase feedback leakage.

2.2.1 Zero-relocation

This method first appeared in (Hartman, 2012). In this method a given non-minimum phase system is represented in controllable canonical form through a coordinate transformation. In the controllable canonical form, the entries in the C matrix are the coefficients of the transfer function numerator for the system. The set of equations in the following show the steps to obtain the controllable canonical matrix \tilde{C} .

Let ABC represent a state space system,

$$H = [B \ A^1B \ A^2B \ \dots \ A^{n-1}B]$$

$$\tilde{A} = H^{-1}AH$$

$$\begin{aligned}
\tilde{A} &= \begin{pmatrix} 0 & 0 & -a_1 \\ 1 & \vdots & \vdots \\ 0 & 1 & -a_n \end{pmatrix} \\
\bar{A} &= \tilde{A}^T \\
\text{Therefore, } \bar{A} &= \begin{pmatrix} 0 & 1 & 0 \\ \vdots & \vdots & 1 \\ -a_1 & \dots & -a_n \end{pmatrix} \\
\bar{B} &= \{0 \quad \dots \quad 1\}^T \\
\bar{H} &= \{\bar{B} \quad \bar{A}^1 \bar{B} \quad \bar{A}^2 \bar{B} \quad \dots \dots \dots \quad \bar{A}^{n-1} \bar{B}\} \\
T &= H \bar{H}^{-1} \\
\bar{C} &= CT
\end{aligned}$$

Once \bar{C} is obtained its entries form the coefficients of the numerator in

$$P(s) = \frac{n(s)}{d(s)} = \frac{c_0 + c_1 s + \dots \dots \dots + c_{n-1} s^{n-1}}{a_0 + a_1 s + \dots \dots \dots + a_{n-1} s^{n-1} + s^n}$$

The numerator in factorized form is:

$$(s + z_1)(s + z_2)(s - z_3) \dots \dots \dots (s + z_{n-1})$$

The above factorization gives the locations of the zeros; the unstable zero is relocated to the left half plane. Let \bar{z}_3 be the new location for the unstable z_3 . Then the numerator of the transfer function changes to $(s + z_1)(s + z_2)(s + \bar{z}_3) \dots \dots (s + z_{n-1})$ with all stable zeros. Since the values are in the controllable canonical form the coefficients of the numerator for the transfer function is the new blended matrix called \bar{C}_b . The following coordinate transformation can be done to obtain the blended C matrix in the original coordinate system $C_b = \bar{C}_b T^{-1}$.

2.2.2 Minimum Phase Feedback Leakage

In this method, a small amount of leakage from a sensor is added to the original output feedback. This can pull the unstable zero into the left half plane. In-depth understanding of system dynamics is required to achieve this. For example if we consider a pitch rate to elevator transfer function, there will always be a zero at the origin because it is a rate term, discussed in detail in Section 4.8. In general, it is good practice to choose a leakage signal which is minimum phase with respect to the input. This method works well for systems with a zero at the origin.

for system output $\underline{y} = C\underline{x}$ and $\underline{y}_A = C_A\underline{x}$

we define the blended output as $\underline{y}_{new} = \underline{y} + L_A\underline{y}_A = \overline{C}\underline{x}$ where $\overline{C}_A \equiv C + L_AC_A$

such that $P(s) = \overline{C}_A(sI - A)^{-1}B$ is minimum phase

Here we see that in order to meet the stability theorem of the direct adaptive control scheme the plant must be strictly dissipative. In linear terms, this maps to a system $G(s)$ being minimum phase with positive high frequency gain. In cases where a plant does not meet the minimum phase requirement we compensate for it with the technique discussed here. We use this non-minimum phase mitigation method to achieve a minimum phase HSV plant in Section 4.

3. HSV MODEL AND SIMULATION OVERVIEW

A first principles nonlinear 3 – *DOF* longitudinal dynamics model of a generic scramjet-powered hypersonic vehicle developed by Bolender, Doman and, Oppenheimer in (Bolender, 2009; Bolender, et al 2007; Bolender, et al 2006; Oppenheimer, et al 2007) is discussed in this section. The vehicle under consideration was developed to study the salient features of a large scale hypersonic cruise or access-to-space vehicle. We use relevant sections of (Korad, 2010) which summarizes the work in (Bolender, 2009; Bolender, et al 2007; Bolender, et al 2007; Bolender, et al 2006; Doman, et al 2006, Oppenheimer, et al 2007) to briefly address the description of the HSV in this section.

The vehicle is 100 feet long, has a mass of 182 slugs and has a first bending mode of roughly 22.6 rad/s (Doman, et al 2006). The control inputs are: elevator, stoichiometrically normalized fuel equivalency ratio (*FER*), diffuser area ratio (not considered in this work), and a canard. The canard was added later on in order to increase the available bandwidth for the controller (Bolender, et al 2006). It should be noted however that a canard may not be physically realizable given the harsh environment in the forward part of the vehicle. For that reason, the HSV model is constructed in a way such that the canard effects can easily be removed. The aircraft may be visualized as shown in Figure 3.1.

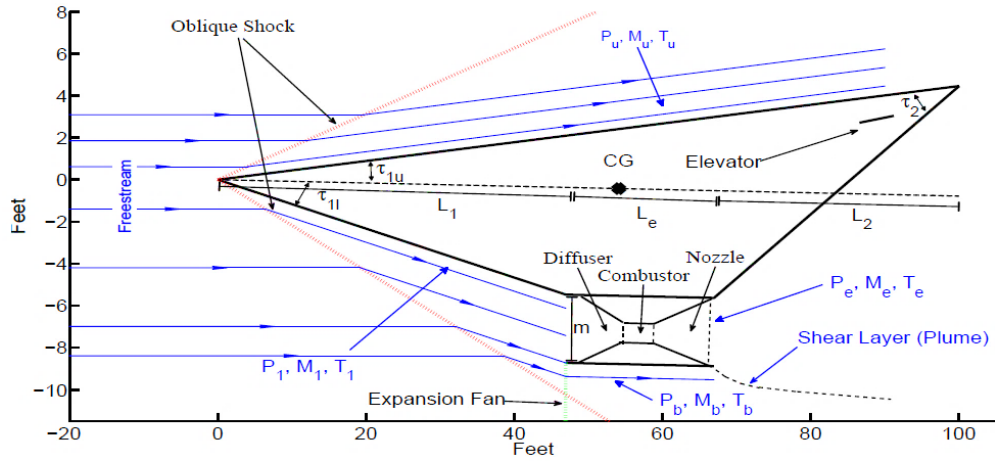


Figure 3.1: Schematic of Hypersonic Scramjet Vehicle (Korad, 2010)

The following sections we briefly discusses the modeling approach.

3.1 Propulsion

The forebody compression ramp provides conditions to the scramjet engine placed in the lower aft end of the body (Bolender, et al 2007). The engine inlet is variable geometry, not considered in the simulation considered in this work. The model assumes the presence of a cowl door, which maintains shock-on-lip condition through AOA feedback also assuming no forebody flexing (Bolender, et al 2006). At cruise condition, the bow shock impinges on the engine inlet (assuming no forebody flexing). At higher or lower speeds the shock angle is either bigger or smaller. If smaller, the shock is captured by the inlet; if bigger, the cowl door reflects it into the engine intake (Bolender, et al 2007), shown in Figure 3.2. Fuel mass flow rate is assumed to be insignificant compared to the air mass flow and for all the range of fuel equivalency ratio (FER) the thrust is assumed to be linear. For values greater than 1, thrust decreases. This phenomenon and shock-shock

interactions are not captured in the model. Reference (Anderson, 2006) discusses such interactions in detail.

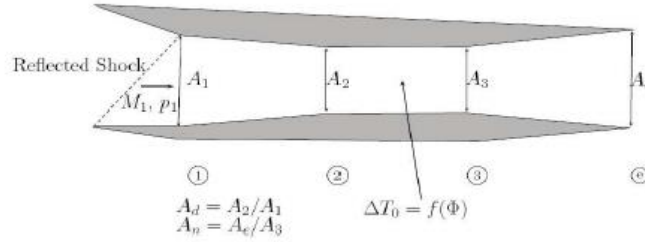


Figure 3.2: Schematic of Scramjet Engine (Korad, 2010)

3.2 Aerodynamics

Prandtl-Meyer theory of expansion and inviscid compressible oblique shock theory are used to calculate the pressure distribution (Korad, 2010). Constant specific heat and specific heat ratio (γ) is assumed to be 1.4. A standard atmosphere model is used, discussed later in this section. Skin friction model or viscous drag effects are based on Eckert's reference temperature method (Bolender, et al 2007); for this the steady state wall temperature is assumed to be 2500 °R after a few minutes of flight. Linear piston theory is used to capture the unsteady effects (Oppenheimer, et al 2007).

3.3 Structures

Effects such as out of plane bending and torsional bending are neglected due to the geometry of the vehicle (i.e. narrow, long and slender) (Doman, et al 2006). A single free-free Euler-Bernoulli beam partial differential equation (infinite dimensional PDE) model is used instead of the Timoshenko beam theory for modeling the longitudinal elasticity of

the vehicle (Oppenheimer, et al 2007). The assumed mode method is used to obtain the natural frequencies ω_n , mode shapes and finite-dimensional approximations. This approach allows the capture of realistic flexible dynamics. Rigid body modes interact and influence the flexible modes through generalized forces (Oppenheimer, et al 2007). It is important to analyze the flexible effects as the flexibility affects the flow field and varies the pressure distribution on the vehicle (Doman, et al 2006; Oppenheimer, et al 2007; Korad, 2010).

3.4 Actuator Dynamics

Simple first order actuator models were used in each of the control channels:

Table 3.1: Actuator Model (Bolender, 2009; Korad, 2010)

Actuator	Model	Input	Output
Elevator	$-\frac{20}{s+20}$	Reference Signal	Deflection Angle
FER	$-\frac{10}{s+10}$	Reference Signal	FER Value
Canard (disabled in this work)	$-\frac{20}{s+20}$	Reference Signal	Deflection Angle

These dynamics did not prove to be critical here. Elevator saturation of $\pm 30^\circ$ is considered, however the adaptive stability augmentation system (SAS) modeled never reached these values. *FER* range of $[0 - 1]$ is used in this work. *FER* is the stoichiometrically normalized fuel equivalency ratio given by $\frac{f}{f_{st}}$, where f denotes the fuel-

to-air ratio and f_{st} denotes the stoichiometric fuel-to-air ratio (Bolender, 2009; Bolender, et al 2007; Korad, 2010). FER is the engine control primarily associated with the vehicle velocity; its impact on the flight path angle is significant since the engine is placed below the vehicle cg (Bolender, et al 2007).

As we will see, the vehicle exhibits both unstable and non-minimum phase dynamics with non-linear aero-elastic-propulsion coupling and critical FER constraint. The linearized model consists of eleven states. Five rigid body states namely speed, pitch, pitch rate, altitude, AOA and six flexible states representing modal coordinates and modal velocities of 3 flexible modes (Bolender, et al 2007; Doman, et al 2006).

3.5 Longitudinal Dynamics

3.5.1 Equations of Motion

The equations of motion for the $3DOF$ flexible vehicle are given as follows (Bolender, et al 2007):

$$\begin{aligned}
 \dot{v} &= \left[\frac{T \cos \alpha - D}{m} \right] - g \sin \gamma \\
 \dot{\alpha} &= - \left[\frac{L + T \sin \alpha}{mv} \right] + q + \left[\frac{g}{v} - \frac{v}{R_E + h} \right] \cos \gamma \\
 \dot{q} &= \frac{M}{I_{yy}} \\
 \dot{h} &= v \sin \gamma \\
 \dot{\theta} &= q \\
 \ddot{\eta}_i &= -2\zeta_i \omega_i \dot{\eta}_i - \omega_i^2 \eta_i + N_i \quad i = 1, 2, 3 \dots \\
 \gamma &\stackrel{\text{def}}{=} \theta - \alpha \\
 g &= g_0 \left[\frac{R_E}{R_E + h} \right]^2,
 \end{aligned}$$

where L denotes lift, T denotes engine thrust, D denotes drag, M is the pitching moment, n_i denotes generalized forces, ζ denotes flexible mode damping factor, ω_i denotes flexible mode undamped natural frequencies, m denotes the vehicle's total mass, I_{yy} is the pitch axis moment of inertia, g_0 is the acceleration due to gravity at sea level, and R_E is the radius of the Earth and h is the geometric altitude.

3.5.2 State Variables

The states consist of five classical rigid body states and six flexible modes states. The rigid states are velocity (v), FPA (γ), altitude (h), pitch rate (q), pitch angle (θ), and the flexible body states ($\eta_1, \dot{\eta}_1, \eta_2, \dot{\eta}_2, \eta_3, \dot{\eta}_3$) (Oppenheimer, et al 2007). These eleven states with the units are summarized in Table 3.2.

Table 3.2: States for Hypersonic Vehicle Model

#	Symbol	Description	Units
1	V	Speed	ft/sec
2	γ	Flight Path Angle	Deg
3	α	Angle of Attack	Deg
4	q	Pitch Rate	Deg/sec
5	h	Altitude	Ft
6	η_1	1 st Flex Mode	-
7	$\dot{\eta}_1$	1 st Flex Mode Rate	Sec ⁻¹

8	η_2	2 nd Flex Mode	-
9	$\dot{\eta}_2$	2 nd Flex Mode Rate	Sec ⁻¹
10	η_3	3 rd Flex Mode	-
11	$\dot{\eta}_3$	3 rd Flex Mode Rate	Sec ⁻¹

3.5.3 Control Variables

The vehicle has three (3) control inputs: a rearward situated elevator δ_e , a forward situated canard δ_c (not considered), and stoichiometrically normalized fuel equivalence ratio (*FER*). These control inputs with the units are summarized in Table 3.3 (Oppenheimer, et al 2007). In this research, we will only consider elevator and *FER*.

Table 3.3: Controls for Hypersonic Vehicle Model

#	Symbol	Description	Units
1	FER	Stoichiometrically normalized fuel equivalency ratio	-
2	δ_e	Elevator deflection	deg
3	δ_c	Canard deflection	deg

Nominal model parameter values for the vehicle under consideration are given in Table 3.4. Additional details about the model may be found in (Bolender, et al 2007; Bolender, et al 2007; Bolender, et al 2006; Doman, et al 2006; Oppenheimer, et al 2007; Sigthorsson, et al 2006).

Table 3.4: Vehicle Nominal Parameter Values (Korad, 2010)

Parameter	Nominal Value
Elevator Position	(-85, -3.5)ft
Diffuser exit/inlet area ratio	1
Titanium Thickness	9.6 in
Center of Gravity	(-55, 0)ft

Figure 3.3 shows the 2-dimensional HSV considered in this work. The longitudinal force and moment analysis is taken as unit depth into the page. The vehicle consists of 4 surfaces: an upper surface (defined by point cf) and three lower surfaces (defined by points cd , gh and ef). All applicable lengths and dimensions are in units of feet and degrees, respectively. Vehicle dimensions are shown in Table 3.5 along with vehicle angles, mass and moment of inertia.

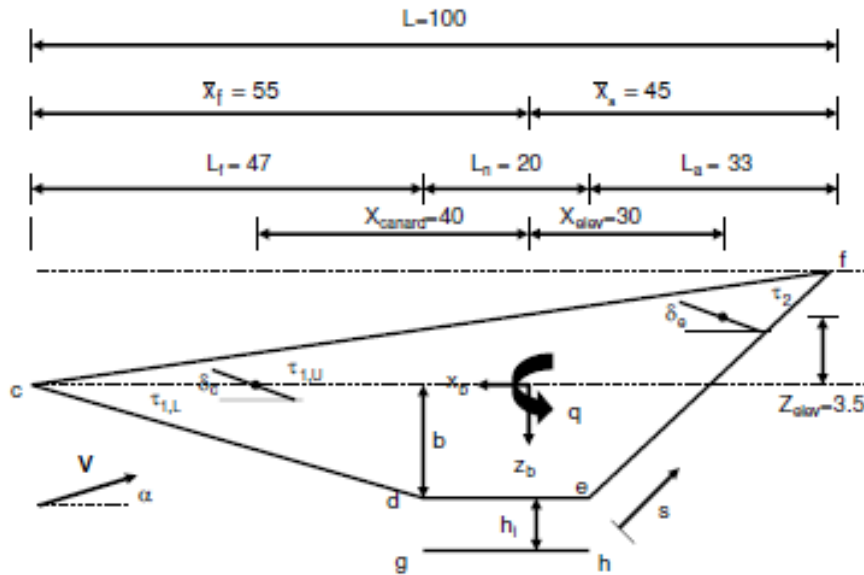


Figure 3.3: Hypersonic Vehicle (Bolender, et al 2007)

Table 3.5: Vehicle Dimensions (Bolender, et al 2007)

L	100 ft	\bar{x}_a	45 ft
L_f	47 ft	x_{elev}	30 ft
L_a	33 ft	h_i	3.25 ft
L_n	20 ft	x_{canard}	40 ft
L_e	17 ft	$\tau_{1,u}$	3°
L_c	10 ft	$\tau_{2,u}$	6°
\bar{x}_f	55 ft	τ_2	14.41°

3.5.4 Summary and Conclusion

In this section, we briefly review the design of the first principles based nonlinear 3-DOF model, for the longitudinal dynamics of the scramjet-powered hypersonic vehicle derived in (Oppenheimer, et al 2007). The model attempts to capture interactions between the aerodynamics, the propulsion system and the flexible dynamics (Doman, et al 2006).

Simplifying assumptions such as neglecting high-temperature gas dynamics, infinitely fast cowl door, no out-of-plane loading, no torsion, no Timoshenko effects, etc. are made. We discuss the dynamic analysis in detail in chapter 4.

3.6 Simulation Overview

The three degree of freedom, physics model derived in (Bolender, et al 2007, Oppenheimer, et al 2007) is coded in Matlab to develop the simulation by Bolender. In this

section we briefly discuss the simulation model, references on this are scarce; thus content of this section are based on the observations made.

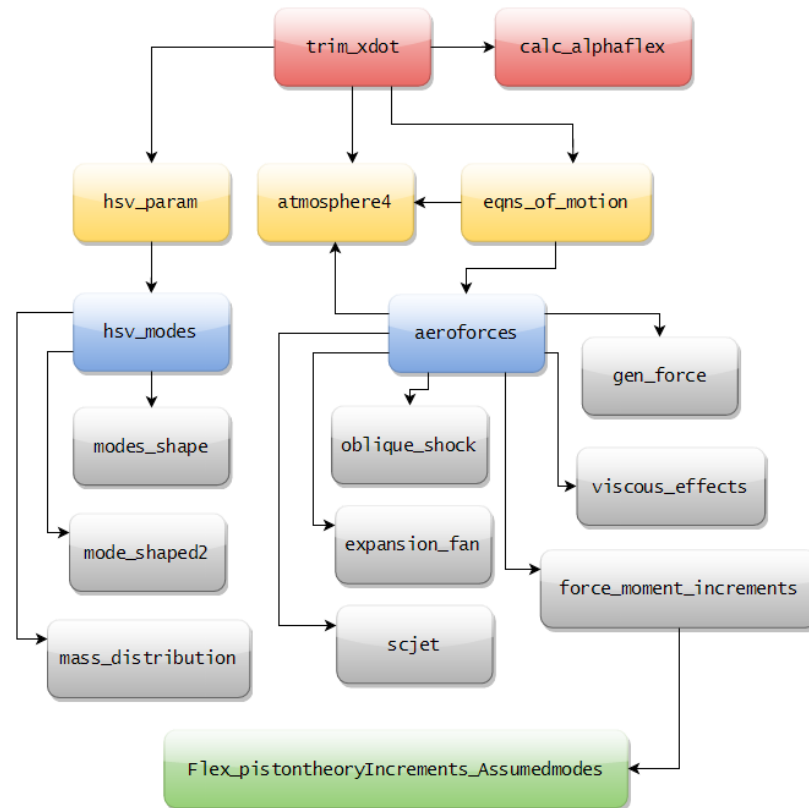


Figure 3.4: Block Diagram Representation of the Nonlinear Model

The model is run through the main code called "trim_xdot". This code loads the aircraft geometry, which is contained in a structure called "ac_param". By default, three flex modes are kept in the model, but five are calculated. It is not recommended to use more than five due to numerical conditioning. The lift, drag, thrust and pitching moment are calculated in the file "xz_generic". This file requires a vector that contains the vehicle geometry. This geometry is defined in the file "hsv_param". When "trim_xdot" is called, it writes this vector to the workspace. Properties such as aircraft's outer mold line or the

mass properties can be edited in this function. The assumed modes approach is coded in “modes_shape” and “mode_shaped2” where the mode shapes/frequencies are calculated. The routine “aeroforces” calculates the pressure, temperature and Mach number after the oblique shocks and the expansion fans for upper and lower surface of the vehicle. The function also computes viscous effects for different sections (upper surface, lower fore body, engine nacelle, rear ramp, elevator and canard) and adds them to find the total viscous lift, drag and moment.

The Matlab code is embedded in a Simulink block as an s-function. The linearizing points are defined in a script and the system is linearized at those operating points to obtain the linearized state-space representation of the system. The linearized state-space representation consists of the following state variables shown in the table below:

Table 3.6: State Variables

State Variables	Symbols (in simulation)	Description
x(1)	V	TAS
x(2)	alpha	AOA
x(3)	q	Pitch rate
x(4)	h	Altitude
x(5)	theta	Pitch angle
x(6)	eta1	Modal coordinate FM1
x(7)	eta1dot	Modal velocity FM1
x(8)	eta2	Modal coordinate FM2
x(9)	eta2dot	Modal velocity FM2

x(10)	eta3	Modal coordinate FM2
x(11)	eta3dot	Modal velocity FM2

and the control variables shown in the following table:

Table 3.7: Controls Variables

State Variables	Symbols (in simulation)	Description
u(1)	delta_e	Elevator Deflection
u(2)	phi	FER

The sim "ndi_flex" contains a simple dynamic inversion control for the flexible system. Running "calc_alphaflex" loads all the necessary parameters for the feedback loops. The sim tracks AoA through a commanded pitch rate. The velocity loop is there for stabilization. The output from this setup is considered to be the baseline performance and is discussed in section 4.4.

At some instances the simulation stops and indicates an error. The reason is that there is a fundamental limitation in either the underlying aerodynamic or propulsion model where it is no longer valid. One common instance is when the engine thermally chokes. The Rayleigh flow model predicts that the Mach number of a supersonic flow decreases with increasing heat addition; therefore, it will ultimately reach a sonic condition where the model is no longer valid. Something similar can occur on the control surface when a larger flow expansion angle is required the model has simply reached a point where it

breaks down. The easiest solution is to be less aggressive with the controlled variables, although with pitch-axis stability and appropriate saturation on the control actuators these instances can be completely removed.

4. ADAPTIVE STABILITY AND COMMAND AUGMENTATION

4.1 Linearization

In this section, the linearization procedure for the HSV model is presented. For a general nonlinear system, we have the following state space representation:

$$\begin{cases} \dot{x}(t) = f(x(t), u(t)) \\ x(0) = x_0 \\ y(t) = g(x(t), u(t)) \end{cases}$$

In order to use the LINMOD command in Matlab, we define the following operating conditions:

- Flight Condition

Dynamic Pressure = 1500 (lbf/ft²)

Altitude = 92000 (feet)

- Vehicle Parameters

Structure containing all the vehicle parameters = *hsv_param*

Function containing earth's atmospheric model calculates the temperature, static pressure and density (rho). Velocity is computed using the equation $\sqrt{\frac{2 \times q}{\rho}}$ and the speed of sound is calculated using the equation $\sqrt{\gamma RT}$.

- Initial Guesses and Constraints Set-Ups for upper and lower surface of the vehicle

$xo = [V \ 0.0314 \ 0 \ 92000 \ 0.0349 \ 0 \ 0 \ 0 \ 0 \ 0 \ 0]$ - States

$uo = [0.157 \ 0.4]$ - Input

$xu0 = [xo; uo]$ - Concatenated Vector

$xL = \text{zeros}(13,1)$ $xU = \text{zeros}(13,1)$

- States

$xL(1) = V$ $xU(1) = V$ - Velocity

$xL(2) = 0$ $xU(2) = 0.0698$ - Angle of Attack

$xL(3) = 0$ $xU(3) = 0$ - Pitch Rate

$$\begin{array}{lll}
 xL(4) = 92000 & xU(4) = 92000 & \text{- Altitude} \\
 xL(5) = 0.0349 & xU(5) = 0.0349 & \text{- Pitch Attitude}
 \end{array}$$

● Flex Mode States

$$\begin{array}{lll}
 xL(6) = -1 & xU(6) = 3 & \text{- Modal Coordinate 1} \\
 xL(7) = 0 & xU(7) = 0 & \text{- Modal Velocity 1} \\
 xL(8) = -1 & xU(8) = 1 & \text{- Modal Coordinate 2} \\
 xL(9) = 0 & xU(9) = 0 & \text{- Modal Velocity 2} \\
 xL(10) = -1 & xU(10) = 1 & \text{- Modal Coordinate 3} \\
 xL(11) = 0 & xU(11) = 0 & \text{- Modal Velocity 3}
 \end{array}$$

● Input States

$$\begin{array}{lll}
 xL(12) = 0 & xU(12) = 0.261 & \text{- Elevator} \\
 xL(13) = 0.1 & xU(13) = 0.6 & \text{- Throttle}
 \end{array}$$

It is desirable to linearize the plant at the trim condition. In this case, the control variables along with the state variables are optimized (minimized) to achieve trimmed level flight. In order to use the optimization function, it is necessary to create an optimization options structure and specify the constraints for the parameters. Following are the values identified by the optimization function:

Table 4.1: Optimized Values for Trim Condition

State Variables	Control Variables
$\mathbf{x} =$ $1.0e + 04 *$ 0.7878 0.0000 0 9.2000 0.0000 0.0001 0 -0.0000 0 -0.0000 0	$\mathbf{u} =$ 0.1836 0.5674

The non-linear model with above state and control variables is trimmed using the Matlab linearization command LINMOD.



Figure 4.1: Aero Model used for Linearization

The following state space representation is obtained:

$$A_{11 \times 11} = \begin{bmatrix} 0 & -17.7 & 0 & 0 & -31.9 & 1.8 & 0 & 1.1 & 0 & 3.7 & 0 \\ 0 & -0.1 & 1 & 0 & 0 & 0 & 0 & 0 & 0 & 0 & 0 \\ 0 & 8.8 & 0 & 0 & 0 & -0.1 & 0 & -0.3 & 0 & -0.1 & 0 \\ 0 & -7878 & 0 & 0 & 7878 & 0 & 0 & 0 & 0 & 0 & 0 \\ 0 & 0 & 1 & 0 & 0 & 0 & 0 & 0 & 0 & 0 & 0 \\ 0 & 0 & 0 & 0 & 0 & 0 & 1 & 0 & 0 & 0 & 0 \\ 0.1 & 7937.6 & 0 & 0 & 0 & -509.6 & -0.8 & -40.7 & 0 & -150.2 & 0 \\ 0 & 0 & 0 & 0 & 0 & 0 & 0 & 0 & 1 & 0 & 0 \\ 0 & -388.2 & 0 & 0 & 0 & 3.2 & 0 & -2531.7 & -2 & 11.7 & 0 \\ 0 & 0 & 0 & 0 & 0 & 0 & 0 & 0 & 0 & 0 & 1 \\ 0 & 636.3 & 0 & 0 & 0 & 1.1 & 0 & -1.8 & 0 & -9753.7 & -4 \end{bmatrix}$$

$$B_{11 \times 2} =$$

$$\begin{bmatrix} -56.3 & 27.2 \\ 0 & 0 \\ -8.7 & 0.2 \\ 0 & 0 \\ 0 & 0 \\ 0 & 0 \\ 2106.2 & 11 \\ 0 & 0 \\ -1435.5 & 38.3 \\ 0 & 0 \\ -133.4 & -33 \end{bmatrix}$$

$$C = I_{11 \times 11}$$

$$D = 0_{11 \times 2}$$

In order to access the requirement of stability and command augmentation on the plant, in the next section we discuss the dynamic analysis conducted in order to understand the various aero and structural modes.

4.2 Dynamic Properties

The nonlinear model is linearized at $M = 8$ and $h = 92,000ft$. We compute the poles and zeros of the linearized plant in order to assess stability and minimum phase characteristics. Poles of the linearized plant are shown in Figure 4.2.

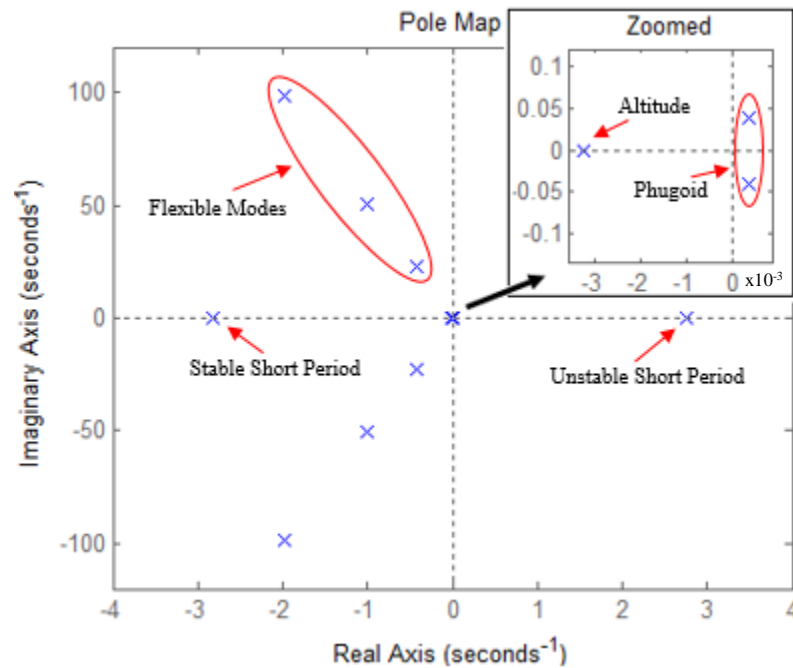


Figure 4.2: Poles of the Plant

Note that the short period mode has both stable and unstable poles. The long forebody and rear mounted engine, typical for hypersonic Waveriders gives them an aft center of gravity, resulting in pitch-up instability.

Table 4.2: Poles location, ω_n and ζ for longitudinal and structural modes

Poles	Damping	Frequency	Mode Name
-1.98E+00 + 9.87e+01i	2.00E-02	9.88E+01	FM3
-1.98E+00 - 9.87e+01i	2.00E-02	9.88E+01	FM3
-1.00E+00 + 5.03e+01i	1.99E-02	5.03E+01	FM2
-1.00E+00 - 5.03e+01i	1.99E-02	5.03E+01	FM2
-4.21E-01 + 2.25e+01i	1.86E-02	2.26E+01	FM1
-4.21E-01 - 2.25e+01i	1.86E-02	2.26E+01	FM1
-2.83E+00 + 0	1.00E+00	2.83E+00	Short Period
2.75E+00 + 0	-1.00E+00	2.75E+00	Short Period
-3.24E-03 + 0	1.00E+00	3.24E-03	Altitude
3.88E-04 + 3.93e-02i	-9.88E-03	3.93E-02	Phugoid
3.88E-04 - 3.93e-02i	-9.88E-03	3.93E-02	Phugoid

In Table 4.2, a closer look at the numerical values of the poles shows us that the system is unstable with unstable short period and phugoid poles. For conventional aircraft, the short period mode is usually heavily damped and has a short period oscillation that occur at nearly constant speed. High frequency and heavy damping are desirable for rapid response to elevator commands without undesirable oscillation and overshoot (Nelson, 1998).

The long period mode represents interchange of potential and kinetic energy about the equilibrium level at constant alpha (Nelson, 1998). The phugoid mode is usually lightly damped, but in our case, the poles are unstable (shown in Table 4.2). Phugoid motion is

almost non-existent in the case of the given hypersonic vehicle. Hypersonic speed and low weight results in a low trade-off between kinetic and potential energy. This characteristic also effects the design of speed augmentation systems; we will discuss this in the following sections.

Table 4.2 also show the characteristics of the structural modes. The flexible modes have a high frequency and low damping, typical of aerospace structures. Results are similar to ones shown in (Bolender, 2009; Bolender, et al 2007; Oppenheimer, et al 2007). Table 4.3 lists the zeros of the linearized model. Notice that the plant is non-minimum phase; this characteristic is a common trend for all tail-controlled aircraft, unless a canard is used (Bolender, et al 2006). Zeros for the transfer function $\frac{q(s)}{\delta_e(s)}$ are shown in Figure 4.3. A single zero at the origin makes the transfer function weakly non-minimum phase. Figure 4.4 shows the zeros for $\frac{v(s)}{\delta_{FER}(s)}$ transfer function. Equation (14) shows that the high frequency gain for this transfer function is negative.

Since the plant is non-minimum phase, in order to meet the requirements of the adaptive stability theorem discussed in Section 2, we modify the sensor arrangement using “sensor blending” which is discussed later in section 4.8.

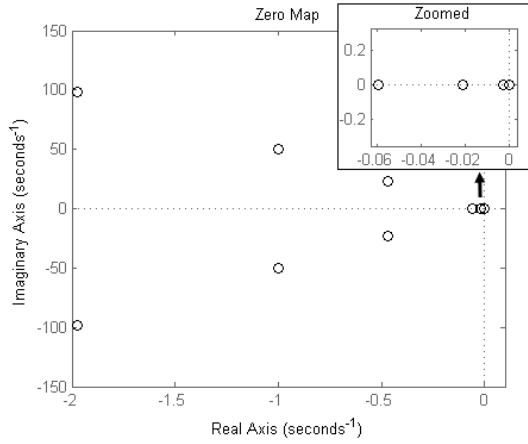


Figure 4.3: Zero map of $\frac{q(s)}{\delta_e(s)}$

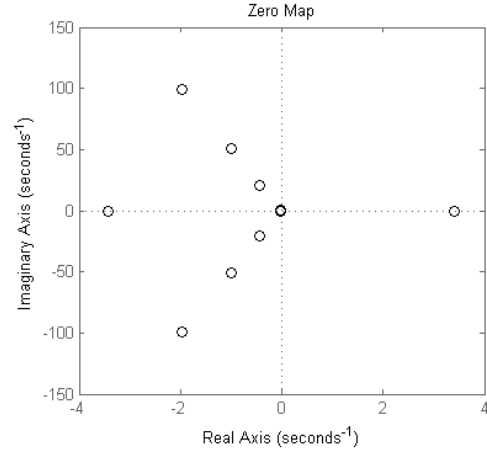


Figure 4.4: Zero Map of $\frac{v(s)}{\delta_{FER}(s)}$

Table 4.3: Zeros for transfer function $\frac{q(s)}{\delta_e(s)}$ and $\frac{v(s)}{\delta_{FER}(s)}$

Transfer Function	Stable/Unstable	Location
$\frac{q(s)}{\delta_e(s)}$	Stable	$-1.9755 \pm 98.7339i$
		$-0.9986 \pm 49.8296i$
		$-0.4659 \pm 22.9452i$
		$-0.0596 + 0$
		$-0.0208 + 0$
		$-0.0028 + 0$
	Marginally Stable	$0 + 0$
$\frac{v(s)}{\delta_{FER}(s)}$	Stable	$-1.9755 \pm 98.7184i$
		$-1.0002 \pm 50.3215i$
		$-0.4208 \pm 22.5611i$
		$-2.8554 + 0$
	Unstable	$2.7824 + 0$

	Stable	-0.0007 + 0.0395i
		-0.0007 - 0.0395i

From the open loop response (Figure 4.5 and Figure 4.6), it is evident that the plant is unstable. Elevator input is set to 0.183 radians and FER is held steady at 0.5674 for this test (trim setting). As soon as the simulation is executed, the vehicle pitches up and goes in a loop across the lateral axis indicating longitudinal instability.

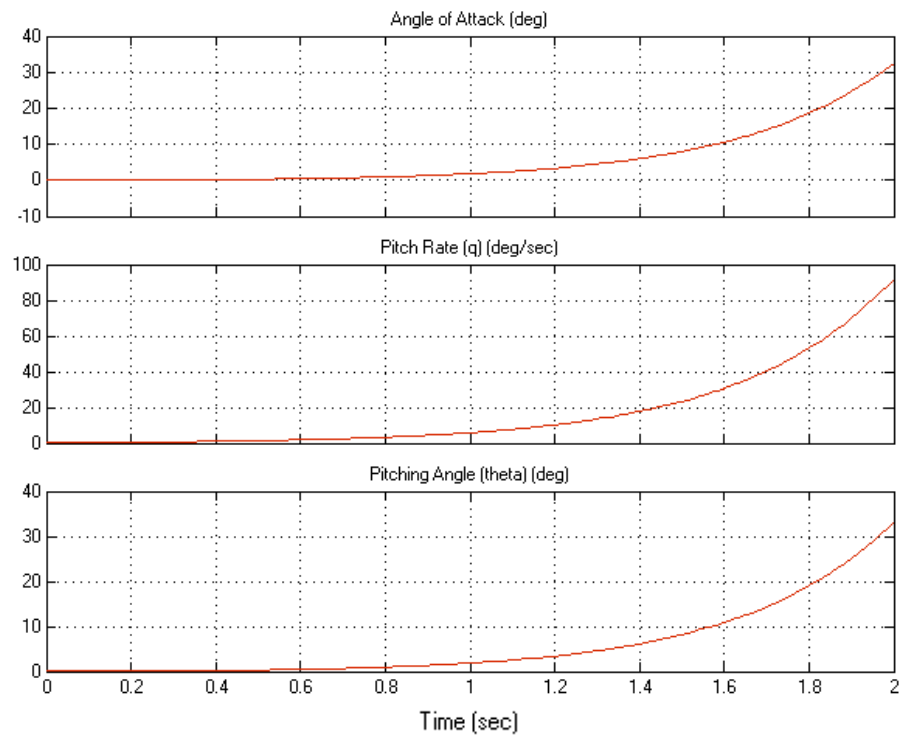


Figure 4.5: Open Loop AOA , q and θ (Incremental Values)

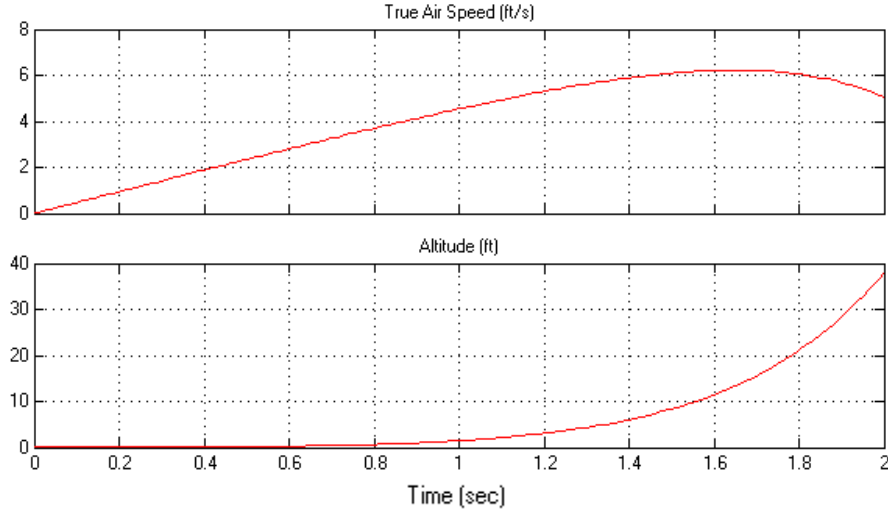


Figure 4.6: Open Loop V and H (Incremental Values)

Thus in order to fix the pitch up instability we propose a stability augmentation system, which is discussed in the next section.

4.3 Pitch-Axis Stability Augmentation

Stability augmentation of an aircraft's dynamics using a feedback control system allows one not only to improve its handling quality characteristics, but also to expand the flight envelope and increase the aircraft's performance characteristics (Hartmann, et al 1979). An aircraft with an aerodynamically unstable configuration, stabilized by a control system can provide higher lift-to-drag ratio, which results in increased endurance (Hartmann, 1979; Ngo, et al 1996; Cameron, et al 2000). Critical flight regimes such as high-incidence departures or aeroelastic instabilities can be significantly relaxed or even eliminated by an active control approach (Friedmann, 1999).

The pitch-axis stability augmentation system provides satisfactory natural frequency and damping for the short-period mode. The short-period mode primarily

involves angle-of-attack and/or pitch rate (Ngo, et al 1996). The feedback of these variables to the elevator input modifies the frequency and damping. The phugoid mode is largely unaffected by this feedback. The outer feedback control loops are usually closed around the pitch SAS to provide autopilot systems (Stevens, et al 1992). The pitching moment curve of a statically unstable aircraft has a positive slope over some or all range of α (Stevens, et al 1992). To generate a restoring pitching moment, perturbation in α are sensed and fed back to the elevator servo to generate a stabilizing pitching moment (Stevens, et al 1992). This makes the slope of the pitching moment curve more negative in the region around the operating AoA.

Due to the vulnerability of the AoA sensor to failure/damage at hypersonic speeds and also due to difficulty in obtaining accurate, quick responding noise-free measurements AoA feedback is usually avoided (Stevens, et al 1992). Thus, we use pitch rate feedback to generate a restoring pitching moment compensation. The pitch-rate sensor is normally a mechanical gyroscopic device, arranged to measure the inertial angular rate around the lateral axis. It is essential to place the gyro in an appropriate location to avoid picking up the vibrations of the aircraft structure (Stevens, et al 1992). Figure 4.7 shows a schematic of a conventional longitudinal pitch-axis stability augmentation control loop.

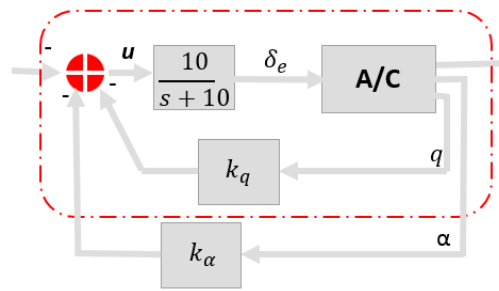


Figure 4.7: General Pitch-Axis Stability Control Loop

4.4 Development of the Pitch-Axis Stability Augmentation

The simulation model consists of a pitch SAS which uses a dynamic inversion control law as mentioned in section 3.6. We analyze the system with this control law; Figure 4.9 shows the closed loop pitch-rate response of the system with the baseline controller. The oscillation amplitude grows over time indicating an unstable closed loop response.

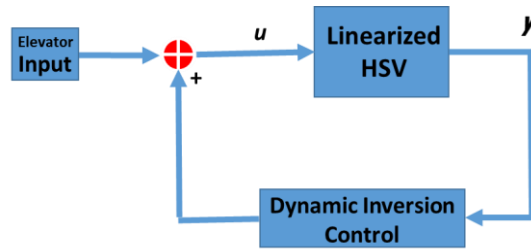


Figure 4.8: Baseline Pitch SAS Control System

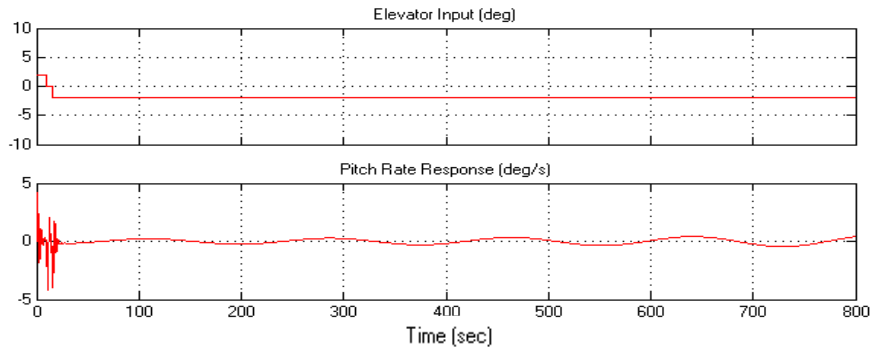


Figure 4.9: Elevator Input and Pitch Rate Response with Dynamic Inversion Controller

In order to test the feasibility of the adaptive control for the given problem, we implement the adaptive control in the outer loop as shown in the figure below, to evaluate improvements (if any) in the pitch rate response.

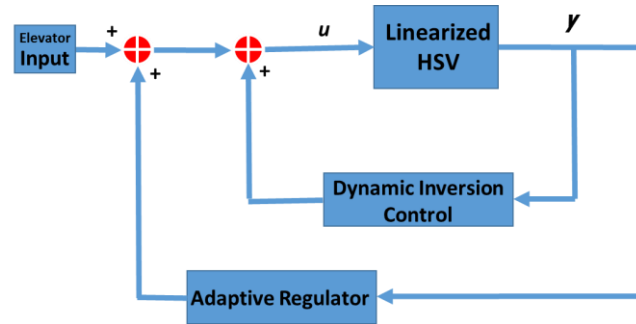


Figure 4.10: Baseline Control with Adaptive Regulator

Figure 4.11 shows the pitch rate response for the same elevator input, the pitch rate damps out stabilizing the plant longitudinally.

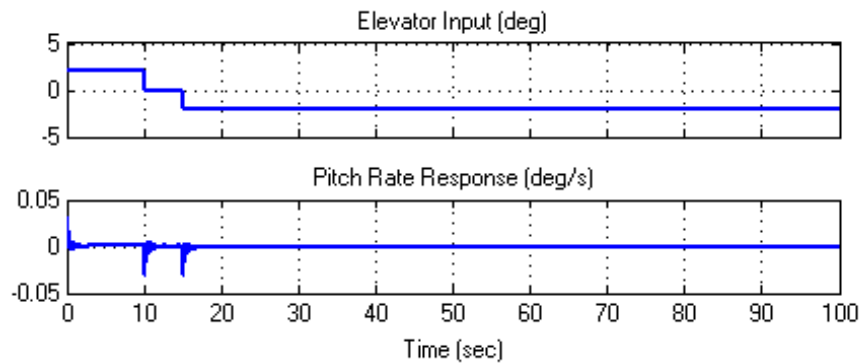


Figure 4.11: Elevator Input and Pitch Rate with Adaptive Regulator

The eleven states flexible model is reduced to a rigid body (five states) model in order to simplify the system by cancelling the structural flexible mode coupling with the longitudinal dynamics. We test the control law with small adjustments on the gain weightings for this simplified system. Figure 4.12 shows that the pitch rate oscillations damp out for the same perturbation.

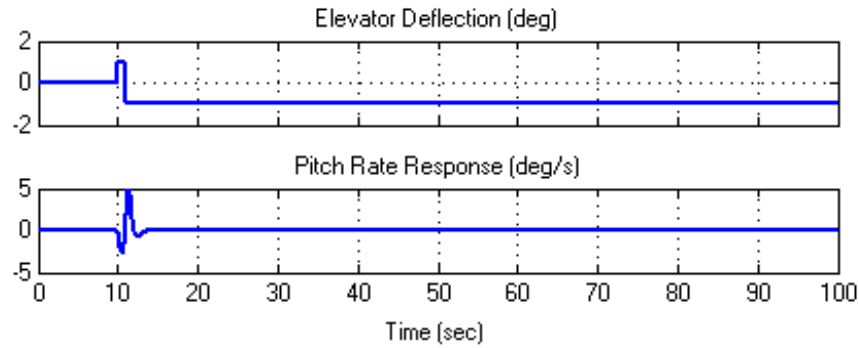


Figure 4.12: Elevator Input and Pitch Rate (Rigid body model)

To satisfy the direct adaptive control scheme's stability theorem we multiply the output feedback by a negative one in order to achieve a positive high frequency gain. Both the simplified rigid body and flexible model are non-minimum phase. We discussed in section 2.2 how non-minimum phase could be alleviated. In the following section, we conduct sensor blending on the system in order to fully satisfy the stability theorem.

The same controller is implemented on the rigid body model of the HSV is implemented on the flexible body model. We see that the control scheme stabilizes the vehicle from the pitch rate response (shown in Figure 4.12).

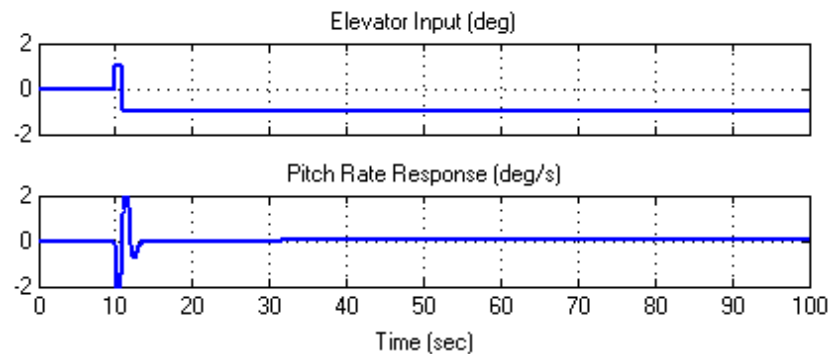


Figure 4.13: Elevator Input and Pitch Rate (Flexible body model)

Figure 4.14 shows the closed loop system for the results obtained in Figure 4.13. Multiplying the output feedback by negative one (shown in Figure 4.14) cancels the negative one shown in equation (21) giving a positive high frequency gain.

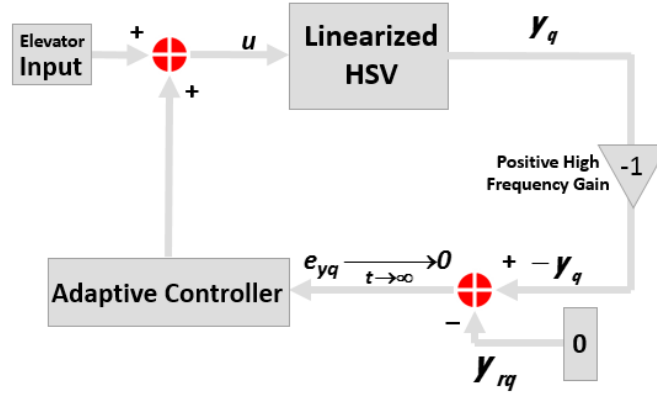


Figure 4.14: δ_e to q loop with adaptive controller for the flexible Model

The numerator for the transfer function $\frac{q(s)}{\delta_e(s)}$ is:

$$q(s) = (-1)[8.749s^{10} + 60.92s^9 + 1.118 \times 10^{-5}s^8 + 3.928 \times 10^{-5}s^7 + 2.686s \times 10^{-8}s^6 + 3.548 \times 10^{-8}s^5 + 1.117 \times 10^{-11}s^4 + 9.287 \times 10^{-9}s^3 + 1.634 \times 10^{-8}s^2 + 3.817 \times 10^{-5}s^1 + 0s^0] \quad (21)$$

Throughout the development of the pitch-axis stability augmentation the *FER* input was set to a constant trim value. In order to track a speed, aircrafts use a system called the Mach-Hold control a type of command augmentation system. The pitch-axis stability augmentation developed in this section serves as a primary inner control system for the development of the Mach-Hold control system. In the following section, we discuss the development of this command augmentation system.

4.5 Mach-Hold by FER Compensation

Mach/Speed-hold is generally used in aircraft with poor longitudinal stability. It is similar to altitude hold in that it is used for cruise condition, and generally involves elevator control, and same inner-loop feedback signals and mixture of fast and slow poles (q and θ) (Stevens, et al 1992). The speed-hold mode maintains constant speed and the vehicle climbs as the vehicle burns fuel. In this mode, throttle position is fixed and generally, speed is controlled by aircraft pitch attitude through operation of the horizontal stabilizer surfaces. A conventional speed-hold control loop schematic is shown in Figure 4.15. Pitch angle output feedback is passed to the controller, which adjusts elevator and the aircraft pitches down or up in order to gain or lose speed respectively. A pitch angle has higher control authority over speed compared to throttle input for aircrafts with low thrust to weight ratio.

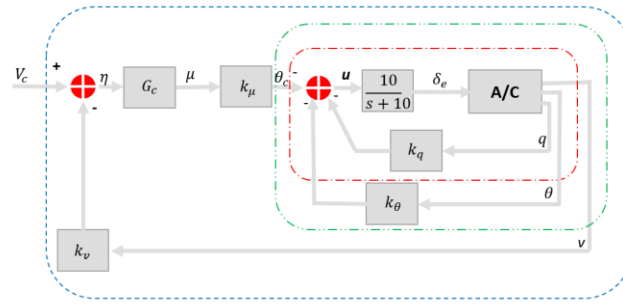


Figure 4.15: General Speed-Hold Control Law

In our case the thrust to weight ratio is greater than one and there is a need to be able to increase speed incrementally for example see mission profile discussed in section 1.3. Thus, considering this we design the Mach-Hold control in order to hold and track commanded speed. In order to achieve this we use the speed output feedback and the

adaptive control scheme generates a FER compensation. In hypersonic aircraft, throttle command has higher control authority on speed over pitch angle. Figure 4.16 shows the proposed Mach-hold and command control loop.

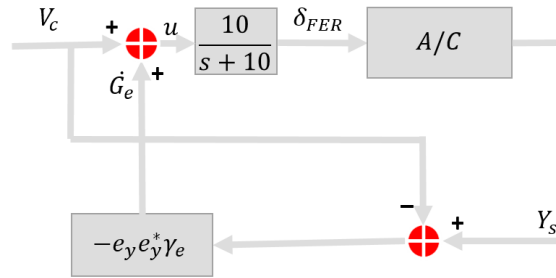


Figure 4.16: Mach-Hold W/ Command Augmentation Proposed

4.6 Mach-Hold Control Development

In order to achieve the goals set in Section 4.5 we design the Mach-Hold control system as an outer loop to the pitch-axis augmentation controller designed in Section 4.4. We implement the Mach-Hold loop shown in Figure 4.17 to the setup shown in Figure 4.14.

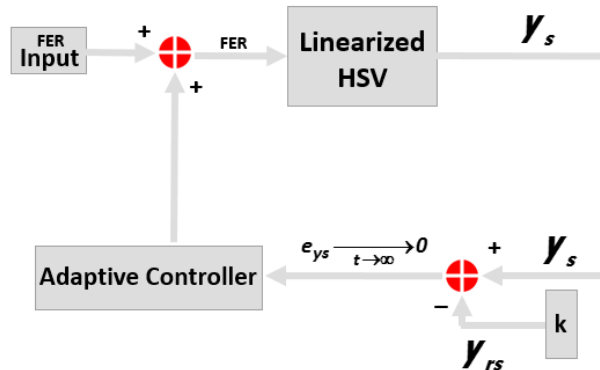


Figure 4.17: FER to v Loop with Adaptive Controller for the Flexible Model

Equation (22) shows the numerator of the transfer function $\frac{v(s)}{\delta_{FER}(s)}$. The $(n - 1)^{th}$ term of the numerator is positive indicating satisfied stability theorem.

$$v(s) = [56.35s^{10} + 387.4s^9 + 7.19 \times 10^{-5}s^8 + 2.456 \times 10^{-6}s^7 + 1.704 \times 10^{-9}s^6 + 2.022 \times 10^{-9}s^5 + 5.944 \times 10^{-11}s^4 + 1.972 \times 10^{-10}s^3 - 7.147 \times 10^{-12}s^2 - 2.89 \times 10^{-11}s^1 - 2.154 \times 10^{-10}s^0] \quad (22)$$

A plot of zeros for the transfer function for *FER* to speed loop is shown in Figure 4.4. The zero on the right half plane makes the *FER* to speed transfer function strongly non-minimum phase. We compensate for the non-minimum phase behavior in the following section through sensor blending.

4.6.1 Simulation Results

To summarize, the system is unstable with non-minimum phase zeros in both the loops. With slight gain weighting adjustments, the model successfully tracks a speed command as illustrated in Figure 4.20 for a given elevator deflection shown in Figure 4.19. From Figure 4.19 and Figure 4.20 we conclude that due to a five deg elevator step input, the plant gains altitude and as a result, the speed should decrease. Instead, the Mach-Hold controller adjusts the *FER* input to hold the initial speed. It should be noted that in Figure 4.19 the *FER* compensation eventually damps out at a value higher than the initial value demonstrating the adjustment made to the input. Figure 4.19 to Figure 4.22 are incremental plots and thus represent the deltas from the trimmed values presented in Table 4.1 in section 3.6. The full control system of two control loops is shown in Figure 4.18.

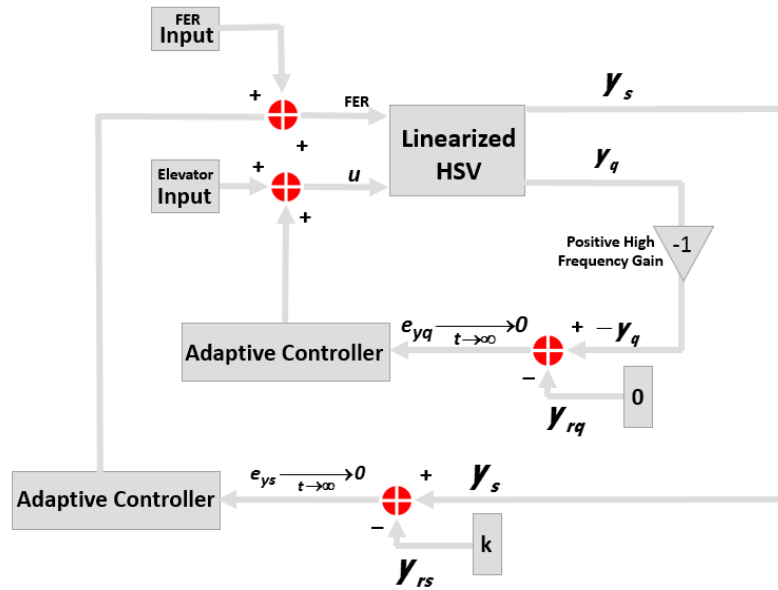


Figure 4.18: Combined FER to v and δ_e to q Adaptive Controller Loops on the Flexible Model

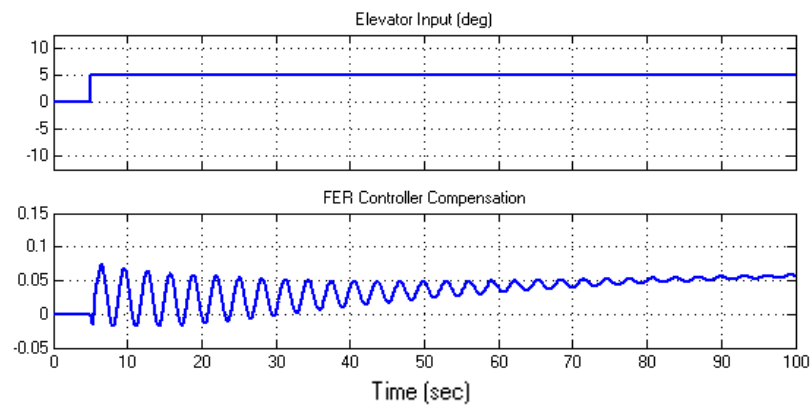


Figure 4.19: Elevator and FER Input

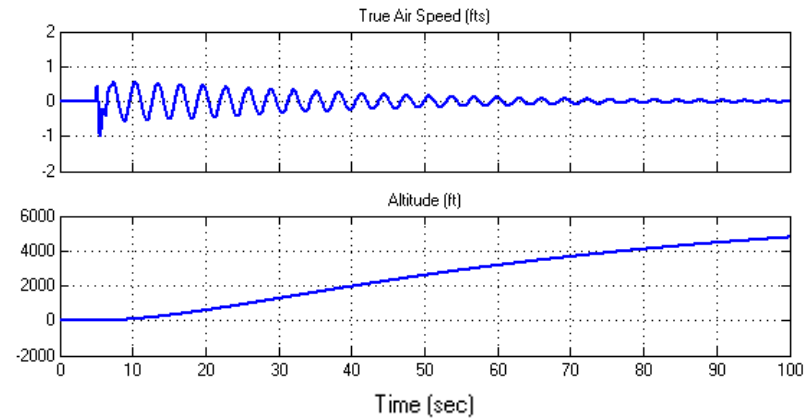


Figure 4.20: Outputs TAS and Altitude

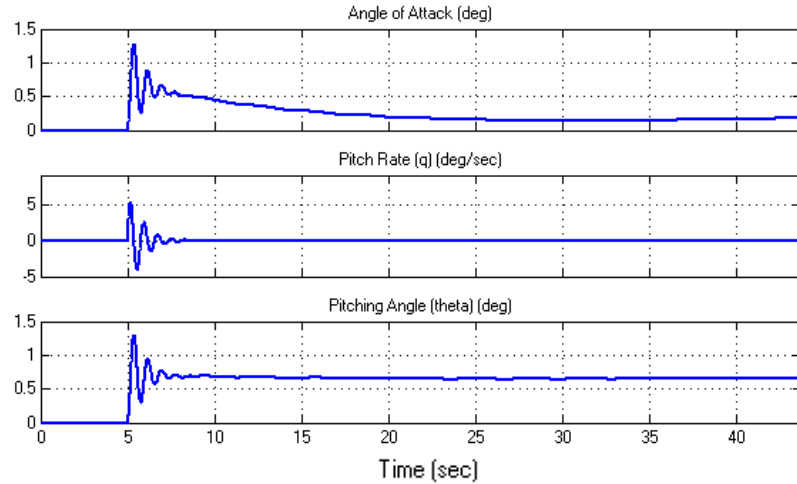


Figure 4.21: AoA, Pitch Rate and Pitch Angle

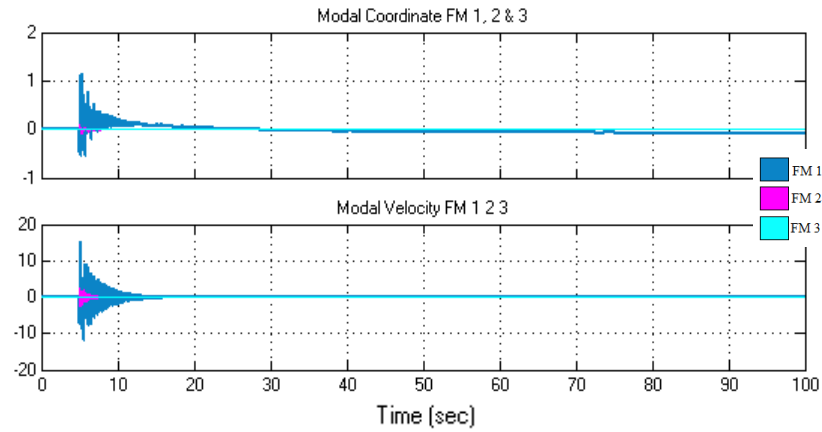


Figure 4.22: Modal Coordinate and Velocity

Figure 4.22 plots the structural flexible modes, the modal coordinates represent the magnitude of bending and the modal velocity denotes the rate of bending. Thus, for any given condition once the vehicle comes to a steady state flight, the modal velocity will always decay to zero whereas the modal coordinate may or may not decay to zero.

In the case presented above, we design a control system in order to track the trim speed and successfully achieve. We modify the control law such that it is possible to

command the speed. Figure 4.23 and Figure 4.24 show the Mach-Hold and Command control loop and the full schematic respectively.

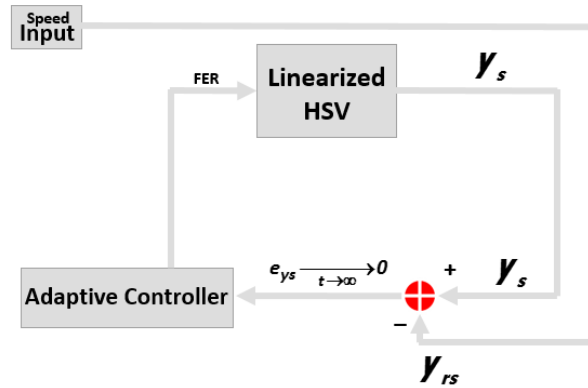


Figure 4.23: Mach-Hold and Command Control System

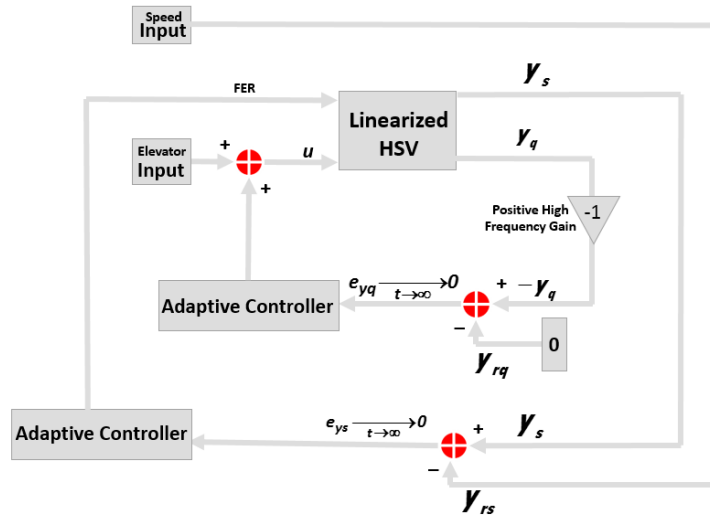


Figure 4.24: Pitch-Axis Stability Augmentation and Mach-Hold and Command Augmentation Control System

We conduct a speed command tracking test on the above closed loop system in order to inspect the control system designed. In Figure 4.25, we can see the incremental speed commands. The Mach-Hold control system adjusts FER to track the commanded

speed. We conduct the test for up to 60 seconds. The powered flight phase (shown in Figure 1.1) of the mission profile consists of similar speed command and lasts up to 200 – 300 seconds.

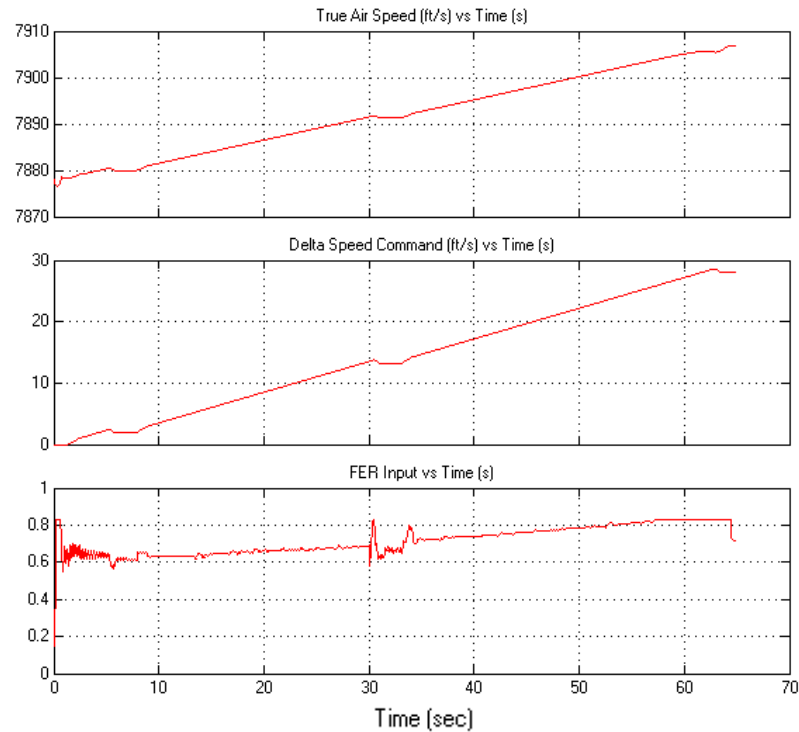


Figure 4.25: TAS, Delta Speed Command and FER Input

4.7 Nonlinear System Application

In this section both the stability augmentation and the command augmentation control systems designed on the linearized plant are implemented on the nonlinear system. The HSV model trimmed at 7878 feet/s and 90,000 feet. Figure 4.27 plots the elevator input time history. In the plots, it should be noted that the elevator is deflected up and down a few times from 0 – 30 seconds. A typical open loop response for the given unstable plant would be growing pitch rate. Here in a closed loop setup, for every elevator input, the adaptive controller compensates accordingly to damp out the pitch rate as shown in Figure

4.28. Throughout these maneuvers, the control system constantly adjusts the FER compensation to track the trimmed speed (shown in Figure 4.27). At 30 seconds, the elevator is deflected and held at five degrees. The pitch-axis stability augmentation loop drives the pitch rate to zero and the vehicle begins to gain altitude as expected (presented in Figure 4.29). The command augmentation loop adjusts FER input to the speed command.

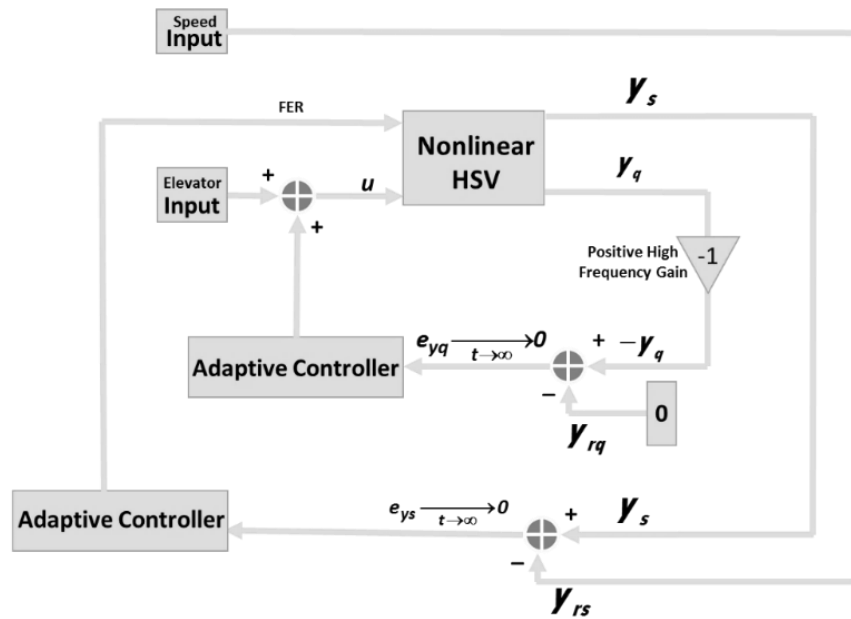


Figure 4.26: Control System on the Nonlinear Model

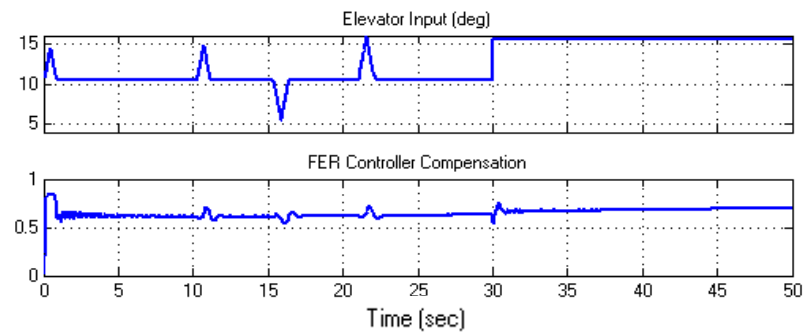


Figure 4.27: Elevator and FER input

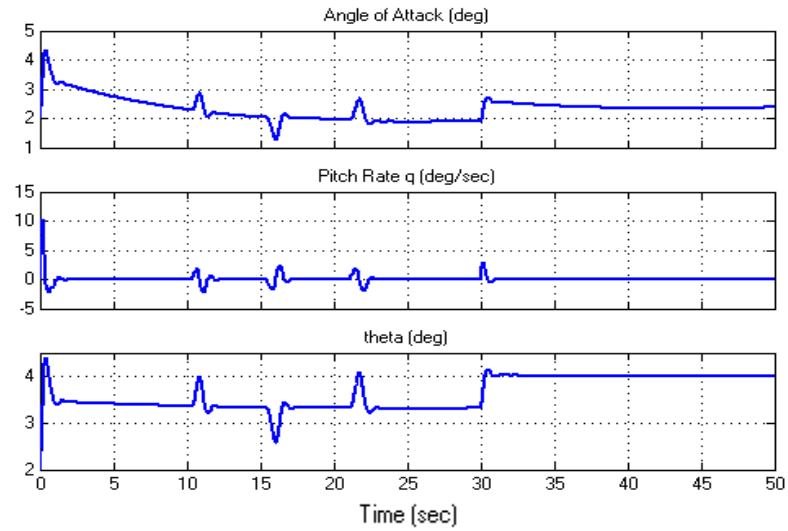


Figure 4.28: AoA, Pitch Rate and Pitch Angle

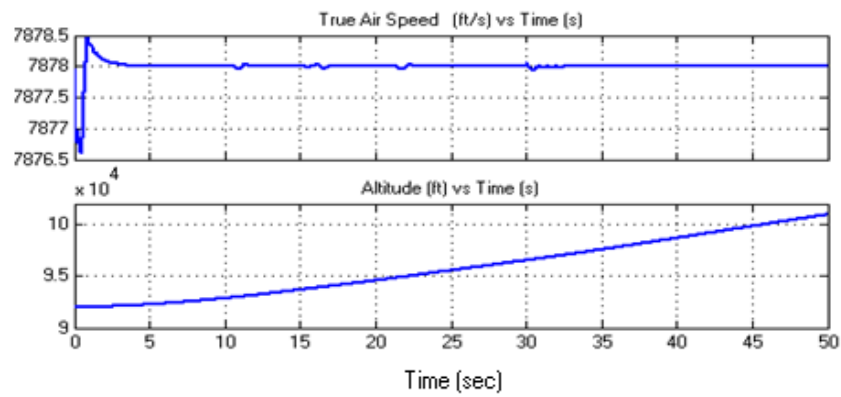


Figure 4.29: TAS and Altitude

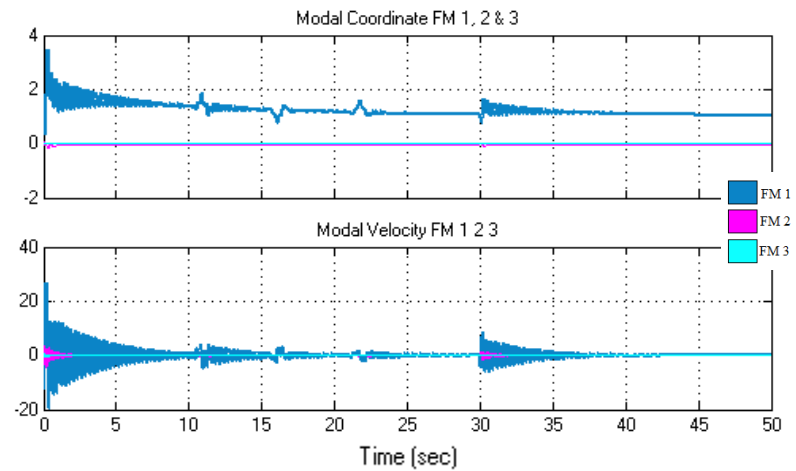


Figure 4.30: Modal Velocity and Coordinate

4.8 Sensor Blending

Although the adaptive controller in both the cases performs very reasonably, the open loop system is still non-minimum phase thus the stability theorem is not satisfied. We use sensor blending on the loops to restore numeric minimum phase. Out of the two different methods discussed in section 2.2, we use minimum phase feedback leakage technique the respective transfer function consists of a zero at the origin.

Table 4.3 shows the numeric values of the zeros for the transfer function $\frac{q(s)}{\delta_e(s)}$ in Section 4.2. The non-minimum phase zero in this transfer function is at the origin. The original C matrix is $C = [0 \ 0 \ 1 \ 0 \ 0 \ 0 \ 0 \ 0 \ 0 \ 0 \ 0]$, the state vector is

$$\underline{x} = [v \ \alpha \ q \ h \ \theta \ \eta_1 \ \dot{\eta}_1 \ \eta_2 \ \dot{\eta}_2 \ \eta_3 \ \dot{\eta}_3]^T$$

A small leakage to the fifth entry representing the signal pitch angle is added. Thus, the new leaked C matrix is $C_l = [0 \ 0 \ 1 \ 0 \ \varepsilon \ 0 \ 0 \ 0 \ 0 \ 0 \ 0]$, where ε is the leakage factor. Here the leakage factor ε is equal to 0.001. Figure 4.31 compares original zero location to the new zero obtained after adding a leakage. The blended C_l matrix is placed in the feedback loop replacing the original C . Figure 4.32 shows the pitch rate response to a pulse elevator input for the unblended setup.

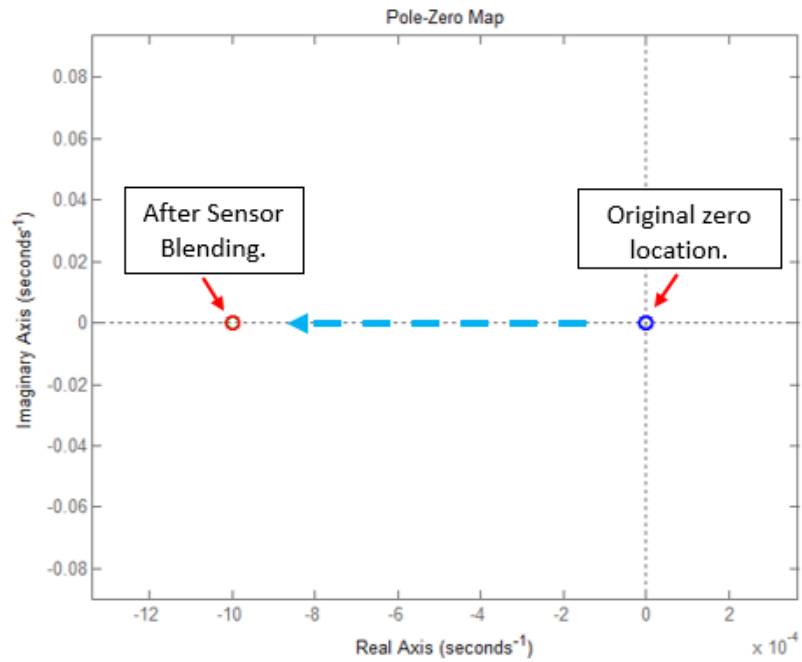


Figure 4.31: Zero Location before and After Sensor Blending

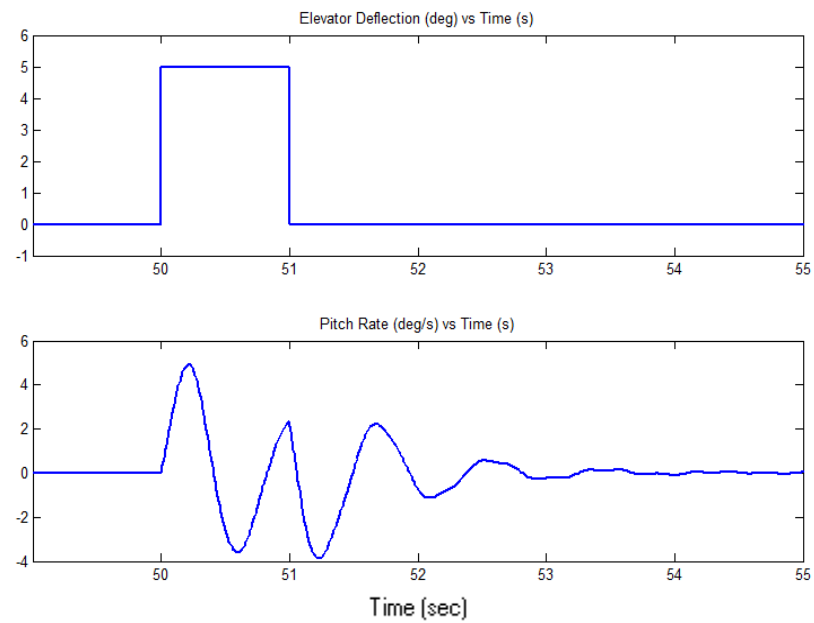


Figure 4.32: Elevator Input and Pitch Rate Response (Unblended System)

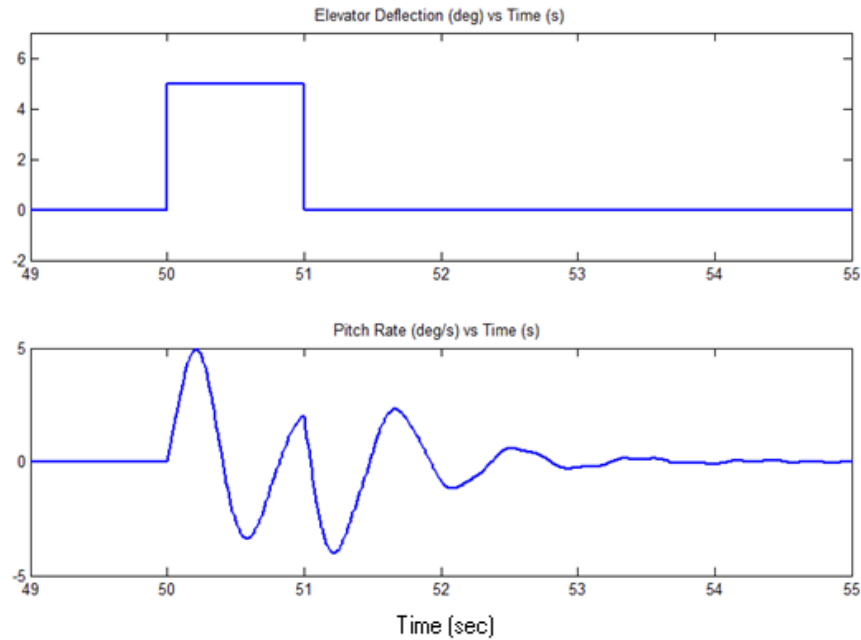


Figure 4.33: Elevator Input and Pitch Rate Response (blended System)

Figure 4.33 shows the pitch rate response to an elevator input for the sensor-blended system. A closer comparison revealed a faster damping in the case of the blended plant. Moreover, the plant meets both the stability theorem requirements (discussed in section 2.1). This guarantees error convergence to zero with bounded adaptive gains.

In the next chapter, we take the multivariable approach and combine the two single input single output loops into one unified multivariable control loop and design a control law using the same control scheme to achieve the same goal of creating a stability and command augmentation system. We compare the results obtained with the SISO setup.

5. MULTIVARIABLE APPROACH

A multivariable system is a system with more than one input and output. Multi Input Multi Output (MIMO) systems bifurcate into two main categories:

- Interactive Systems (non-diagonal transfer function matrix)

$$\begin{aligned}\dot{\underline{x}} &= \begin{bmatrix} a & m & 0 \\ d & b & k \\ 0 & e & b \end{bmatrix} \underline{x} + \begin{bmatrix} q & w \\ r & e \\ t & y \end{bmatrix} \underline{u} \\ \underline{y} &= \begin{bmatrix} a & s & d \\ f & g & h \end{bmatrix} \underline{x}, \text{ assuming no feed through}\end{aligned}$$

- Non-interactive Systems (diagonal transfer function matrix)

$$\begin{aligned}\dot{\underline{x}} &= \begin{bmatrix} a & \cdots & 0 \\ \vdots & b & \vdots \\ 0 & \cdots & b \end{bmatrix} \underline{x} + \begin{bmatrix} q & w \\ r & e \\ t & y \end{bmatrix} \underline{u} \\ \underline{y} &= \begin{bmatrix} a & s & d \\ f & g & h \end{bmatrix} \underline{x}, \text{ assuming no feed through}\end{aligned}$$

In a MIMO plant with input m and output l , the basic transfer function model is $y(s) = G(s)u(s)$, where $\mathbf{y} \in R^l$, $\mathbf{u} \in R^m$ and $G(s)$ is an $l \times m$ transfer function matrix. When a change in one input, u_1 affects more than one outputs from a given set of outputs; y_1, y_2, \dots, y_l the plant is called an interactive system (Skogestad, et al 2005). For a non-interacting plant, u_1 will only affects y_1 , u_2 will only affects y_2 , and so on.

5.1 Control Scheme in Multivariable Setup

In case of a SISO setup we already know that the stability theorem requires positive high frequency gain (*i.e.* $CB > 0$) and minimum phase. However, this does not precisely apply to a multivariable plant since $CB \in R^{n \times n}$, n being the number of inputs and the

outputs. A multivariable system can be broken down into n^2 transfer functions, where each transfer functions can have unique set of zeros. This creates a need for a more precise definition of zeros in the case of a multivariable plant. In addition, since CB is a vector and not a scalar, it should be symmetric and positive definite for a multivariable system to satisfy the direct adaptive control scheme's stability theorem. It should be noted that CB may not be symmetric and positive definite. In these situations, the C matrix has to be blended in order to achieve those conditions. We discuss the definition of multivariable transmission zeros in the following section.

5.2 Multivariable Zeros

As for SISO systems, it is known that RHP-zeros impose fundamental limitations on control, and its definition is clearly stated and understood. Skogestad and Postlethwaite in [60] describe the multivariable zeros as the values of $s = z$ where $G(s)$ loses rank. However, this definition may fail in case of an incorrect pole zero cancellation where the poles and zeros have same location but different direction.

Skogestad and Postlethwaite (Skogestad, et al 2005) also describe the multivariable zeros as poles of $G^{-1}(s)$. The set of zeros obtained through this definition contain all the multivariable zeros. Extraneous zeros \cup transmission zeros \equiv Multivariable zeros; it should be noted that the set of extraneous zeros may be empty.

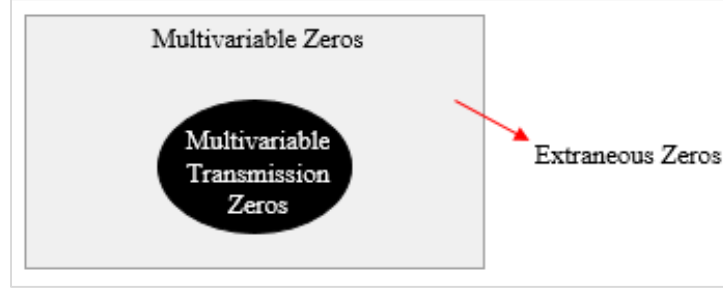


Figure 5.1: Multivariable Zeros

For the given HSV system, this seem to be the case. However, as per the requirements we only need to assure that the multivariable transmission zeros are stable.

Thus, from Hespanha's definition in (Hespanha, 2009) a multivariable transmission zero is the value of λ which completely blocks the input signal and outputs a zero showing a transmission blocking property, thus we refer to them as blocking zeros as well in this work. In more formal terms multivariable zeros are all the values of λ_* for which $y = 0$ in system (A, B, C) with input signal $u = e^{\lambda_* t}$ or

$$Z(A, B, C) \equiv \{ \lambda \text{ such that } H(\lambda) \equiv \begin{bmatrix} A - \lambda I & B \\ C & 0 \end{bmatrix} : \text{is singular} \}$$

For example if we assume the system $A = \begin{pmatrix} 0 & 1 \\ 0 & 0 \end{pmatrix}, B = \begin{bmatrix} 0 \\ 1 \end{bmatrix}, C = [1 \ 1]$. Then \Rightarrow

$$H(\lambda) \begin{bmatrix} \lambda & -1 & 0 \\ 0 & \lambda & 1 \\ 1 & 1 & 0 \end{bmatrix} \Rightarrow \det(H(\lambda)) = -\lambda - 1. \text{ Therefore } Z(A, B, C) = \{-1\}.$$

Based on this definition we discuss ways of computing these multivariable transmission zeros. In order to compute the transmission zeros we obtain the normal form (Balas, et al 2016) of the given system. Normal form is a coordinate transformation to

obtain a matrix \bar{A} , such that $\bar{A} = \begin{bmatrix} \bar{A}_{11} & \bar{A}_{12} \\ \bar{A}_{21} & \bar{A}_{22} \end{bmatrix}$, where all the multivariable transmission zeros are the eigenvalues of the matrix \bar{A}_{22} . We discuss the zeros computed through this method in the following section.

5.2.1 Multivariable Zeros

We compute the multivariable zeros for the definition in (Hespanha, 2009).

Table 5.1: SISO Zeros vs Multivariable Zeros

Zeros	Elevator to Pitch Rate	FER to Speed	Multivariable Zeros
1	$-1.9755 + 98.7339i$	$-1.9755 + 98.7184i$	$-1.9755 + 98.7033i$
2	$-1.9755 - 98.7339i$	$-1.9755 - 98.7184i$	$-1.9755 - 98.7033i$
3	$-0.9986 + 49.8296i$	$-1.0002 + 50.3215i$	$-0.9984 + 49.8332i$
4	$-0.9986 - 49.8296i$	$-1.0002 - 50.3215i$	$-0.9984 - 49.8332i$
5	$-0.4659 + 22.9452i$	$-0.4208 + 22.5611i$	$-0.4688 + 23.0660i$
6	$-0.4659 - 22.9452i$	$-0.4208 - 22.5611i$	$-0.4688 - 23.0660i$
7	$-0.0596 + 0.0000i$	$-2.8554 + 0.0000i$	$-0.0617 + 0.0000i$
8	$-0.0208 + 0.0000i$	$2.7824 + 0.0000i$	$-0.0206 + 0.0000i$
9	$-0.0028 + 0.0000i$	$-0.0007 + 0.0395i$	$0.0000 + 0.0000i$
10	$0.0000 + 0.0000i$	$-0.0007 - 0.0395i$	

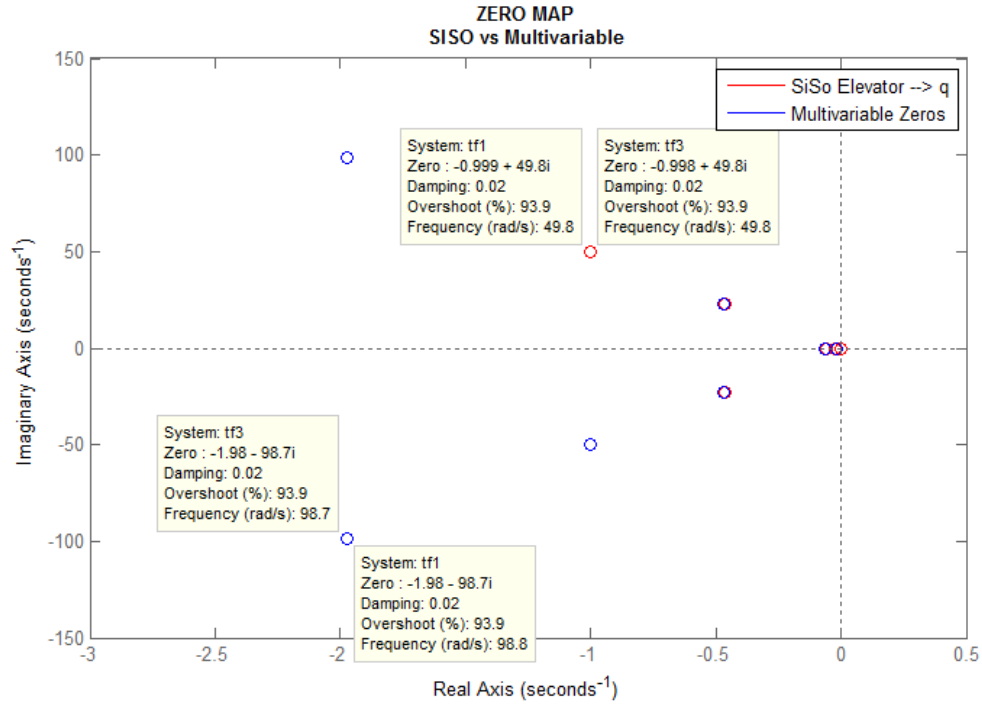


Figure 5.2: Zeros of $\frac{q(s)}{\delta_e(s)}$ vs Multivariable Zeros Overlay

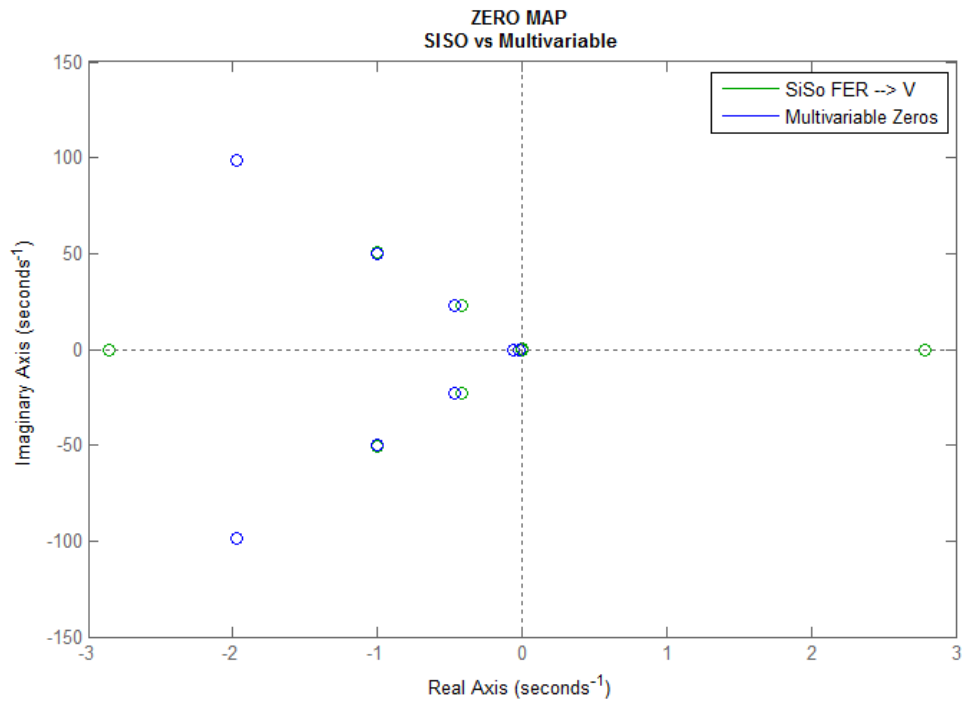


Figure 5.3: Zeros of $\frac{v(s)}{\delta_{FER}(s)}$ vs Multivariable Zeros Overlay

It should be observed that the set of multivariable zeros does not contain any zero with $Re(\lambda) > 0$, shown in Table 5.1 and Figure 5.3. Thus, the set of multivariable transmission zeros also should not contain any such non-minimum phase zeros, since the set of multivariable transmission zeros are contained in the set of multivariable zeros. A possible reason could be pole zero cancellation or the multivariable dynamics. In this work we do not investigate the cause of this, since it is only required to know if the multivariable transmission zeros are stable. In the next section, we discuss the normal form technique in detail and present the zeros obtained through this computation.

5.2.2 Multivariable Transmission Zeros

Computation through normal form: In this technique we conduct a coordinate transformation and look for values of lambda for which outputs are zero, see (Balas, et al 2016).

Assume the open loop system is:

$$\begin{cases} \dot{\underline{x}} &= A\underline{x} + B\underline{u} \\ \underline{y} &= C\underline{x}; \underline{x}(0) = \underline{x}_0 \in X \end{cases} \quad (23)$$

Let the dimension of $\underline{y} = \underline{x} = R^m$ and assume the determinant of $CB \neq 0$.

$$\text{Let } \begin{bmatrix} \underline{y} \\ \underline{z} \end{bmatrix} = \begin{bmatrix} C_{m \times n} \\ W_{2r \times n} \end{bmatrix} \underline{x} \ni (r \equiv n - m)$$

$$\Rightarrow \underline{x} = \begin{bmatrix} C \\ W_2 \end{bmatrix}^{-1} \begin{bmatrix} \underline{y} \\ \underline{z} \end{bmatrix}$$

$$\text{assuming } \begin{bmatrix} C \\ W_2 \end{bmatrix}^{-1} = Q = [Q_1 Q_2]$$

$$\Rightarrow \begin{bmatrix} \dot{\underline{y}} \\ \dot{\underline{z}} \end{bmatrix} = \begin{bmatrix} C \\ W_2 \end{bmatrix} \dot{\underline{x}} = \begin{bmatrix} C \\ W_2 \end{bmatrix} [A\underline{x} + B\underline{u}]$$

Therefore:
$$\begin{bmatrix} \dot{\underline{y}} \\ \underline{z} \end{bmatrix} = \begin{bmatrix} c \\ w_2 \end{bmatrix} A[Q_1 Q_2] \begin{bmatrix} \underline{y} \\ \underline{z} \end{bmatrix} + \begin{bmatrix} c \\ w_2 \end{bmatrix} B \underline{u}$$
 (24)

Now let:
$$\begin{bmatrix} c \\ w_2 \end{bmatrix} A[Q_1 Q_2] = \bar{A} = \begin{bmatrix} \bar{A}_{11} & \bar{A}_{12} \\ \bar{A}_{21} & \bar{A}_{22} \end{bmatrix} \text{ and}$$

$$\begin{bmatrix} c \\ w_2 \end{bmatrix} B = \bar{B} = \begin{bmatrix} CB \\ 0 \end{bmatrix} \quad (25)$$

$$\Rightarrow \underline{y} = C \underline{x} = \underbrace{C[Q_1 Q_2]}_{\bar{C}} \begin{bmatrix} \underline{y} \\ \underline{z} \end{bmatrix} = [I_m \ 0] \begin{bmatrix} \underline{y} \\ \underline{z} \end{bmatrix} \quad (26)$$

We solve for $W_2, Q_1, Q_2 \ni W_2 B = 0; C Q_1 = I_m; C Q_2 = 0$ (27)

With equations from (23) - (27) the following theorem is proved in (Balas, et al 2014).

Theorem: Let CB be non-zero. Then $X = \mathbb{R}^N = R(B) \oplus N(C)$ where $P_1 \equiv B(CB)^{-1}C$ and $P_2 \equiv I - P_1$ are non-orthogonal projections onto $R(B)$ and $N(C)$ respectively.

It can also be proved that $N(C) = R(P_2) = sp\{\theta_1 \dots \dots \theta_r\}$, where $\theta_1 \dots \dots \theta_r$ are basis of columns of P_2 . These linearly independent columns can be ortho-normalized to get $\{\phi_1, \dots, \phi_r\}$, which span $N(C)$.

Define $Q_2 \equiv \begin{bmatrix} \phi_1 & \dots & \phi_r \end{bmatrix}_{r \times r}$

$$Q_2^* Q_2 = \begin{bmatrix} Q_1^* \\ Q_r^* \end{bmatrix} [\phi_1 \dots \phi_r] = I_r \text{ and}$$

$$\begin{aligned} C Q_2 &= C [\phi_1 \dots \dots \phi_r] \\ &= [C \phi_1 \dots \dots C \phi_r] = [0 \dots \dots 0] = 0 \text{ Since } \phi_k \in N(C) \end{aligned}$$

In addition, defining: $Q_1 \equiv B(CB)^{-1} \Rightarrow C Q_1 = CB(CB)^{-1} = I_m$ and

$$W_2 \equiv Q_2^* P_2$$

$$\Rightarrow W_2 B = Q_2^* P_2 B = Q_2^* (0) = 0$$

Since, $P_2 B = (I - P_1) B = B - B = 0$. Now, it can be proved that

$$Q = \begin{bmatrix} c \\ w_2 \end{bmatrix}^{-1} = [Q_1 Q_2]$$

Thus in normal form:

$$\begin{cases} \dot{\underline{y}} &= \bar{A}_{11} \underline{y} + \bar{A}_{12} \underline{z} + CB\underline{u} \\ \dot{\underline{z}} &= \bar{A}_{21} \underline{y} + \bar{A}_{22} \underline{z} \end{cases}$$

$$\text{Where } \bar{A} = \begin{bmatrix} \bar{A}_{11} & \bar{A}_{12} \\ \bar{A}_{21} & \bar{A}_{22} \end{bmatrix} = \begin{bmatrix} C \\ W \end{bmatrix} A \begin{bmatrix} Q_1 & Q_2 \end{bmatrix} = \begin{bmatrix} CAB(CB)^{-1} & CA \overbrace{[\phi_1 \dots \phi_r]}^{Q_2} \\ Q_2^* P_2 AB(CB)^{-1} & \underbrace{Q_2^* P_2 A Q_2}_{\bar{A}_{22}} \end{bmatrix}$$

It can be proved that $\bar{A}_{22} = [(\phi_K, P_2 A \phi_l)]_{r \times r}$ is equal to $[Q_2^* P_2 A Q_2]$ and that W_2 is an isometry on $N(C)$. We can finally prove that the zero dynamics transfer function of the system is $\bar{A}_{12}(sI - \bar{A}_{22})^{-1}\bar{A}_{21}$

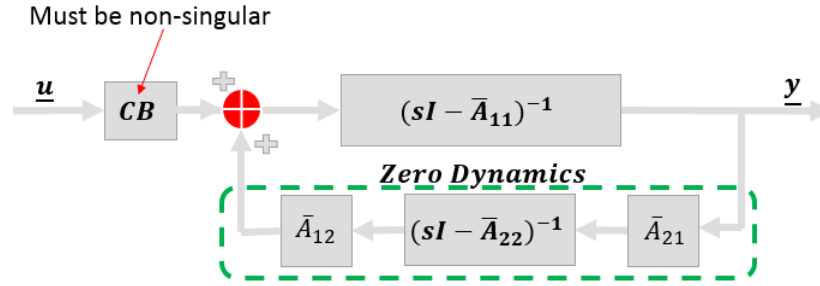


Figure 5.4: System in Normal Form

Definition: $\lambda_* \in \mathbb{C}$ is a blocking zero of (A, B, C) when $H(\lambda_*) = \begin{bmatrix} A - \lambda_* I & B \\ C & 0 \end{bmatrix}$ is singular, i.e. $N(H(\lambda_*)) \neq \{0\}$. This allows proving that $\forall CB$ non-singular $\mathbb{Z}(A, B, C) \equiv \{\lambda_* \in \mathbb{C} \mid H(\lambda_*) \text{ singular}\} = \{\text{eigenvalues of } \bar{A}_{22}\}$ (Balas, et al 2016).

In order to compute the transmission zeros using this method CB of the system must be non-singular. From theory, it is known that P_1 and P_2 are non-ortho-normal projections on $R(B)$ and $N(C)$. Therefore, the first step is to calculate P_1 and P_2 .

$$P_1 = B(CB)^{-1}C, \quad P_2 = I - P_1 \quad (28)$$

The next step is to ortho-normalize the basis of P_2 which spans the null space of C . The newly obtained vectors form the matrix Q_2 . We calculate the matrix \bar{A}_{22} using the following equation

$$\bar{A}_{22} = Q_2^* P_2 A Q_2 \quad (29)$$

Eigenvalues of \bar{A}_{22} give the multivariable transmission zeros for the given system. In Table 5.2, we show the multivariable transmission zeros computed through normal form.

Table 5.2: Multivariable Zeros Set VS Transmission Zeros Set

	Multivariable Zeros (<i>for A,B,C,D</i>)	Multivariable Transmission Zeros (<i>for A,B,C_t,D</i>)
1	$-1.9755 + 98.7033i$	$-2.59 - 1.1089i$
2	$-1.9755 - 98.7033i$	$-2.59 + 1.1089i$
3	$-0.9984 + 49.8332i$	$-0.78 - 0.3314i$
4	$-0.9984 - 49.8332i$	$-0.78 + 0.3314i$
5	$-0.4688 + 23.0660i$	$-0.14 - 0.1554i$
6	$-0.4688 - 23.0660i$	$-0.14 + 0.1554i$
7	$-0.0617 + 0.0000i$	$-0.06 + 0.0000i$
8	$-0.0206 + 0.0000i$	$-0.02 + 0.0000i$
9	$0.0000 + 0.0000i$	$0.0000 + 0.0000i$

Note: The C matrix for the above computation is adjusted such that the matrix CB is invertible, symmetric and positive definite in order to satisfy the stability theorem. As predicted in section 5.2.1 the set of multivariable zeros also does not contain any $Re(\lambda) > 0$ non-minimum phase zeros, but it does contain a zero at the origin.

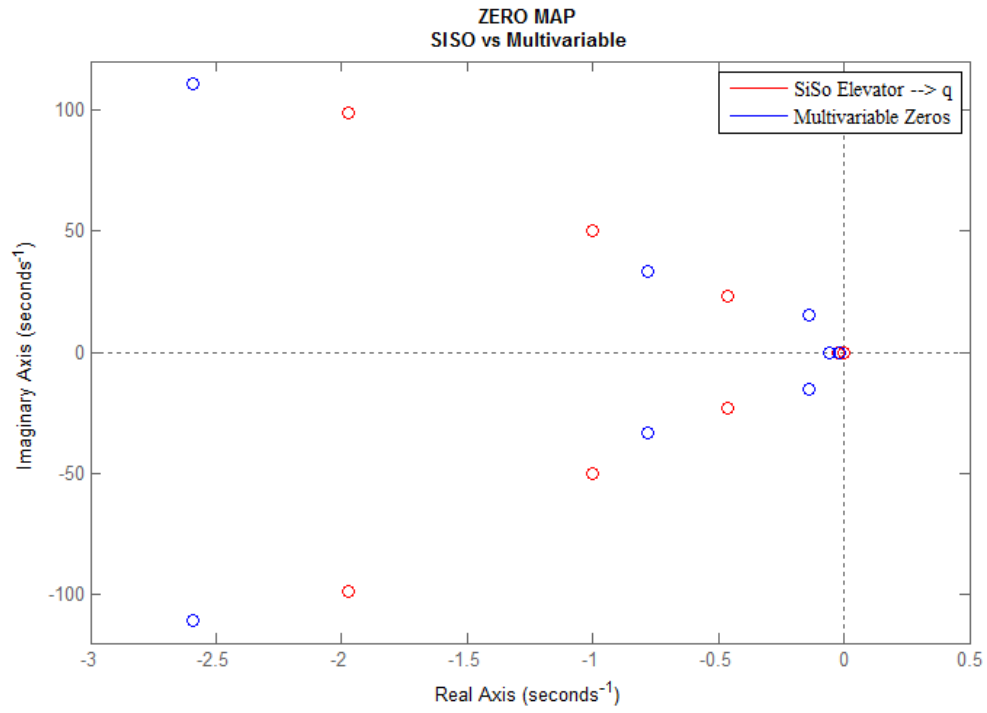


Figure 5.5: Zeros of $\frac{q(s)}{\delta_e(s)}$ vs Multivariable Transmission Zeros Overlay

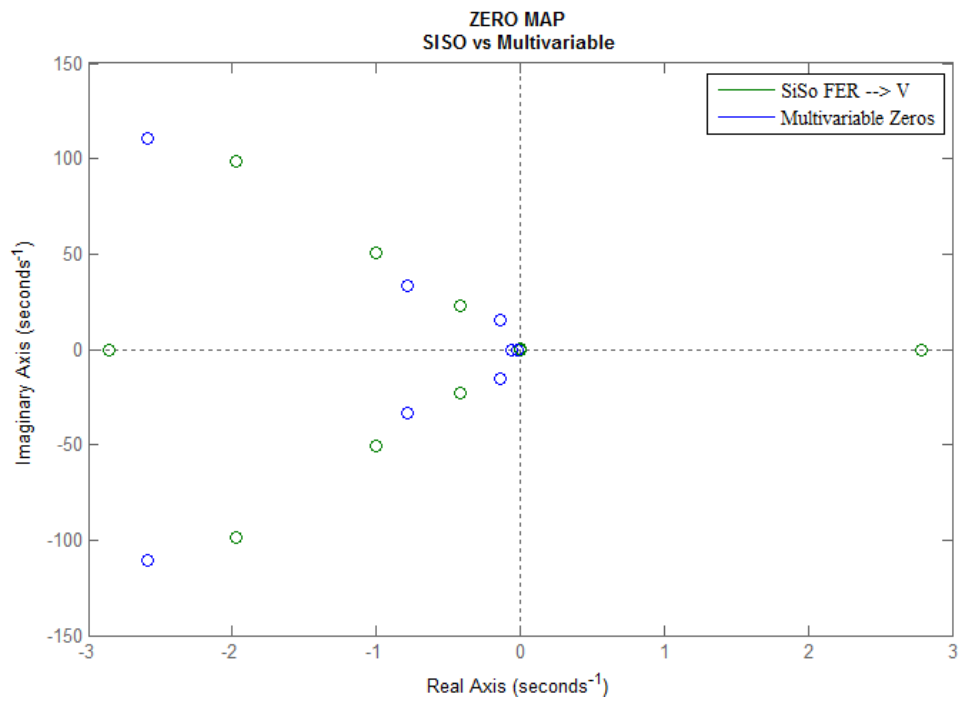


Figure 5.6: Zeros of $\frac{v(s)}{\delta_{FER}(s)}$ vs Multivariable Transmission Zeros Overlay

It should be noted that the set of multivariable transmission zeros does not contain any strongly non-minimum phase zero “satisfying the stability theorem requirement”. In the following section, we discuss the implementation of the control scheme on the multivariable plant and discuss some of the results obtained.

5.3 Multivariable Direct Adaptive Control

We briefly go over the stability theorem requirements of the control scheme.

- Matrix CB symmetric, positive definite
- $\mathbb{Z}(A, B, C) \equiv \{\lambda \in \mathbb{C} \mid \text{Re } \lambda < 0\}$

The plant meets both the requirements except for the one zero at the origin. It should be noted that this could be easily compensated by using a zero filter as discussed in (Balas, et al 2016). Multivariable zeros for the HSV system with δ_e and δ_{FER} as input signals, v , and q as system output signals are computed using the normal form in section 5.2.2. We list these zeros and compare them with the zeros of the SISO system.

Table 5.3: SISO vs Transmission Zeros Comparison

Zeros	Elevator to Pitch Rate	FER to Speed	Transmission Zeros (for A, B, C, D)
1	$-1.9755 + 98.7339i$	$-1.9755 + 98.7184i$	$-2.59 - 1.1089i$
2	$-1.9755 - 98.7339i$	$-1.9755 - 98.7184i$	$-2.59 + 1.1089i$
3	$-0.9986 + 49.8296i$	$-1.0002 + 50.3215i$	$-0.78 - 0.3314i$
4	$-0.9986 - 49.8296i$	$-1.0002 - 50.3215i$	$-0.78 + 0.3314i$
5	$-0.4659 + 22.9452i$	$-0.4208 + 22.5611i$	$-0.14 - 0.1554i$

6	$-0.4659 - 22.9452i$	$-0.4208 - 22.5611i$	$-0.14 + 0.1554i$
7	$-0.0596 + 0.0000i$	$-2.8554 + 0.0000i$	$-0.06 + 0.0000i$
8	$-0.0208 + 0.0000i$	$2.7824 + 0.0000i$	$-0.02 + 0.0000i$
9	$-0.0028 + 0.0000i$	$-0.0007 + 0.0395i$	$0.0000 + 0.0000i$
10	$0.0000 + 0.0000i$	$-0.0007 - 0.0395i$	

As noted previously, there are no transmission zeros with $Re(\lambda) > 0$ in the multivariable system compared to the SISO system. We apply the control scheme on the HSV system in a setup shown in the figure below, in order to provide artificial pitch-axis stability and speed-hold and command control. In Figure 5.8, we show the time history of the inputs δ_e and δ_{FER} made to the system. Figure 5.11 shows the pitch rate response, implying correct compensation by the control law in order to maintain longitudinal stability. With these results, it is evident that the control scheme provides the appropriate elevator compensation using the pitch rate output feedback.

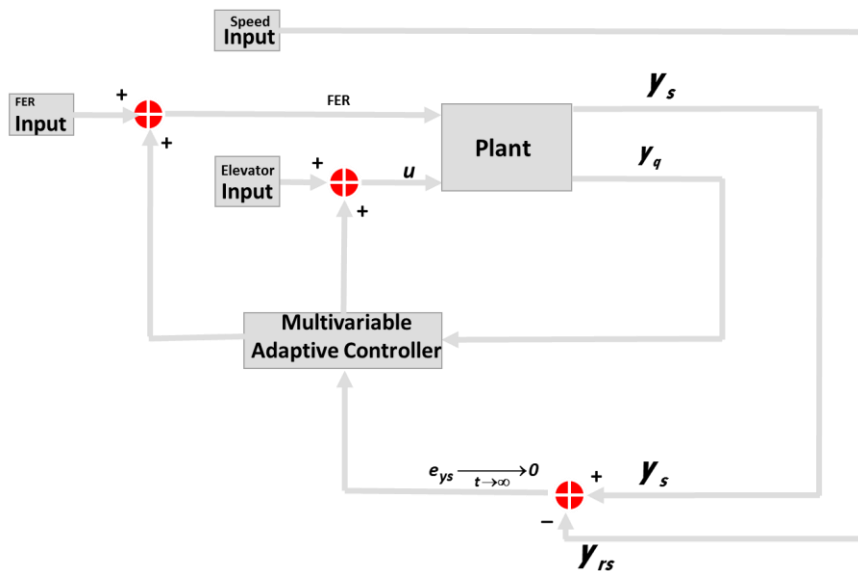


Figure 5.7: Multivariable System and Control System

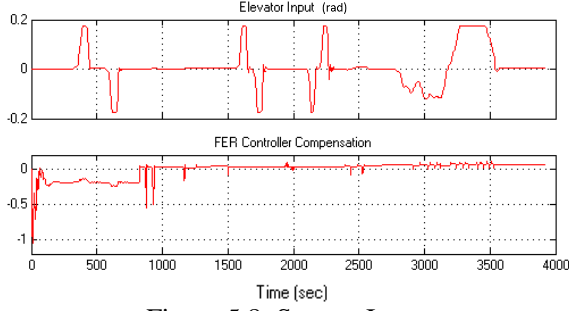


Figure 5.8: System Inputs

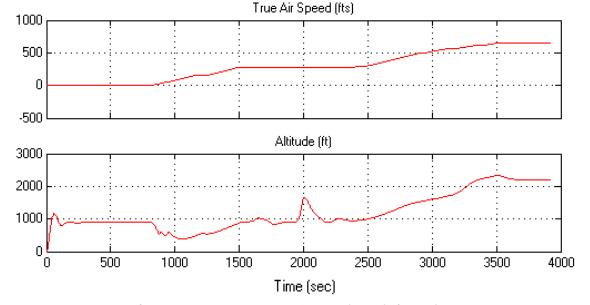


Figure 5.9: TAS and Altitude

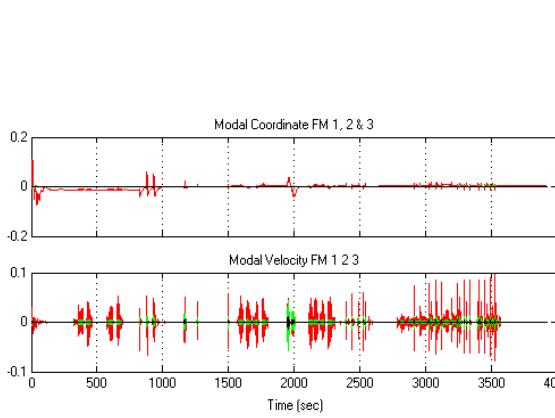


Figure 5.10: Modal Coordinate and Velocity

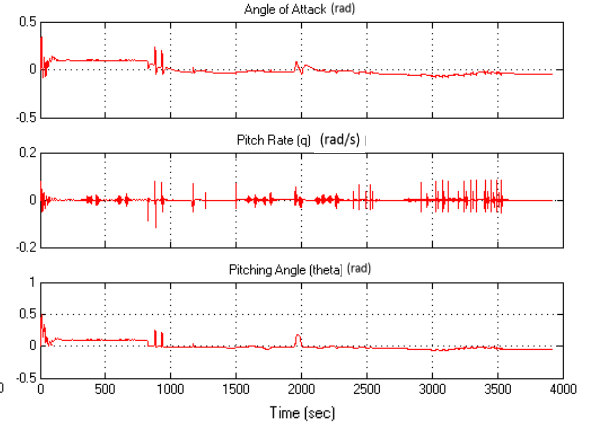


Figure 5.11: System Output

In the next section, we observe the system response to different gain weightings in the coupling terms.

5.4 Coupling Gain Weightings

In this section, we manipulate the coupling terms in the gain-weighting matrix and compare the plots for the following elevator input. The coupling terms in the gamma-e weighting matrix are named k_1 and k_2 for referencing. The term k_1 multiplies with the error $-e_v e_v^*$ and generates a compensation for elevator. Thus, increasing k_1 will increase the compensation produced for elevator for a change in FER input. The term k_2 multiplies

with the error $-e_q e_q^*$ and generates a compensation for FER . Thus increasing k_2 will increase the compensation produced for FER for a change in elevator input. In the first case, we set the coupling weightings $k_1 = k_2 = -0.001$ and set up the following input signal shown in Figure 5.12 as the standard input for all the cases.

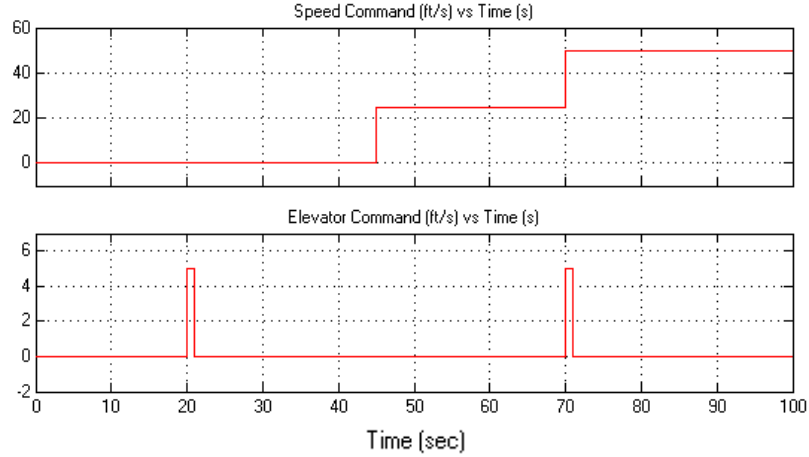


Figure 5.12: Input Command Speed and Elevator Deflection for Test Cases

We set $k_1 = k_2 = -0.001$ as the baseline case and test the following weightings:

Table 5.4: Coupling Weightings

	k_1	k_2
Baseline	0.001	0.001
Case 1	0.001	100
Case 2	100	0.001
Case 3	100	100

The baseline case has the smallest cross coupling and the output signal should be close to the SISO system response. We compare the pitch rate response and speed command

tracking to identify the best coupling weightings. It can be observed that for larger weightings on k_1 speed tracking and pitch rate response are very poor, shown in Figure 5.13. We can see that the speed tracking error grows for case 2 but converges to zero for the baseline case. We see a similar trend for case 3 shown in Figure 5.14.

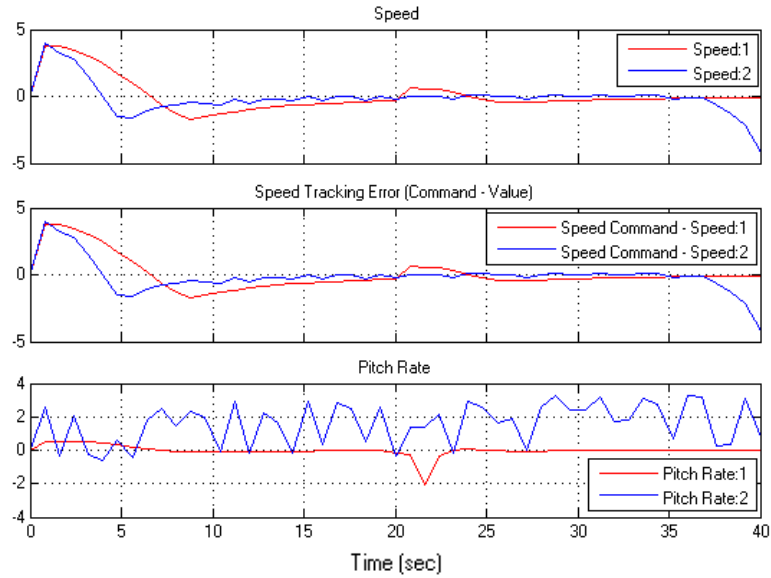


Figure 5.13: Speed, Speed tracking error and pitch rate (Red - Baseline, Blue - Case 2)

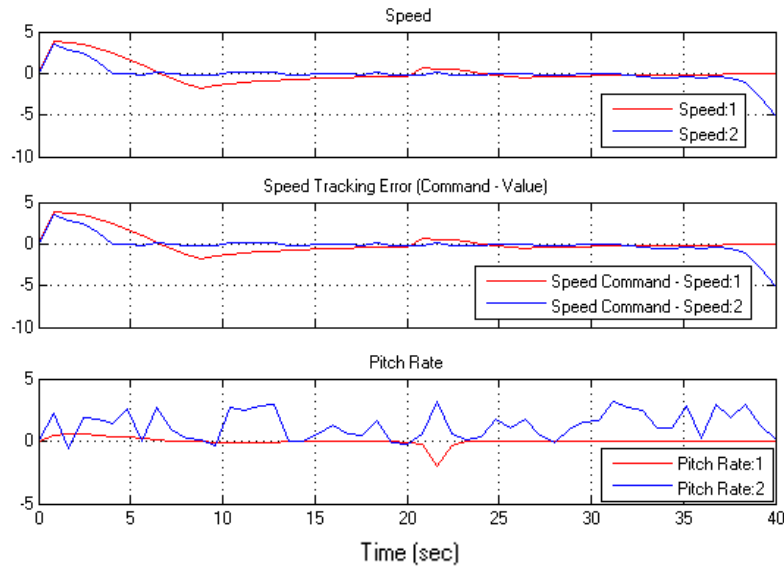


Figure 5.14: Speed, Speed tracking error and pitch rate (Red - Baseline, Blue - Case 3)

In case 1, the response is similar to the baseline response shown in Figure 5.15. A close look reveals better convergence in case 1. From this, we can conclude that the high weightage on FER compensation deteriorates the performance.

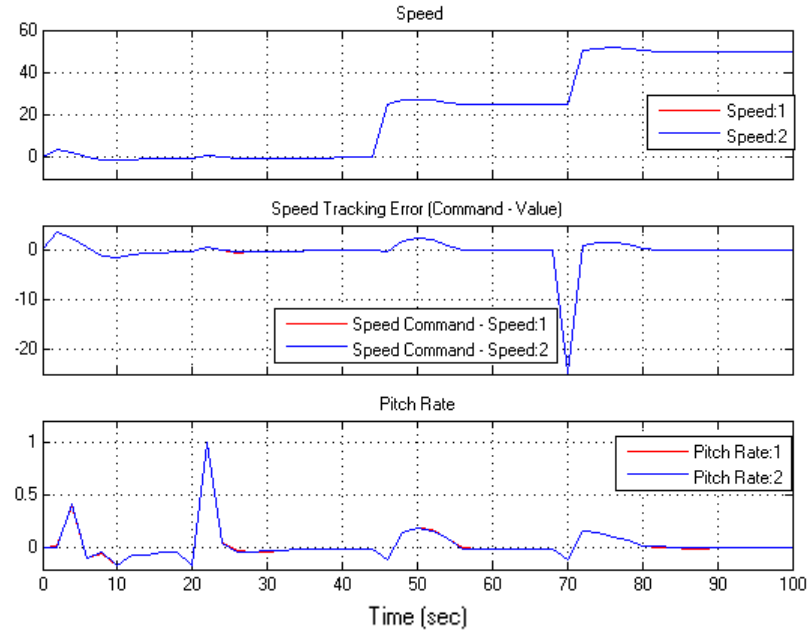


Figure 5.15: Speed, Speed tracking error and pitch rate (Red - Baseline, Blue - Case 1)

Lastly, we compare the SISO system response with the MIMO case 1 response.

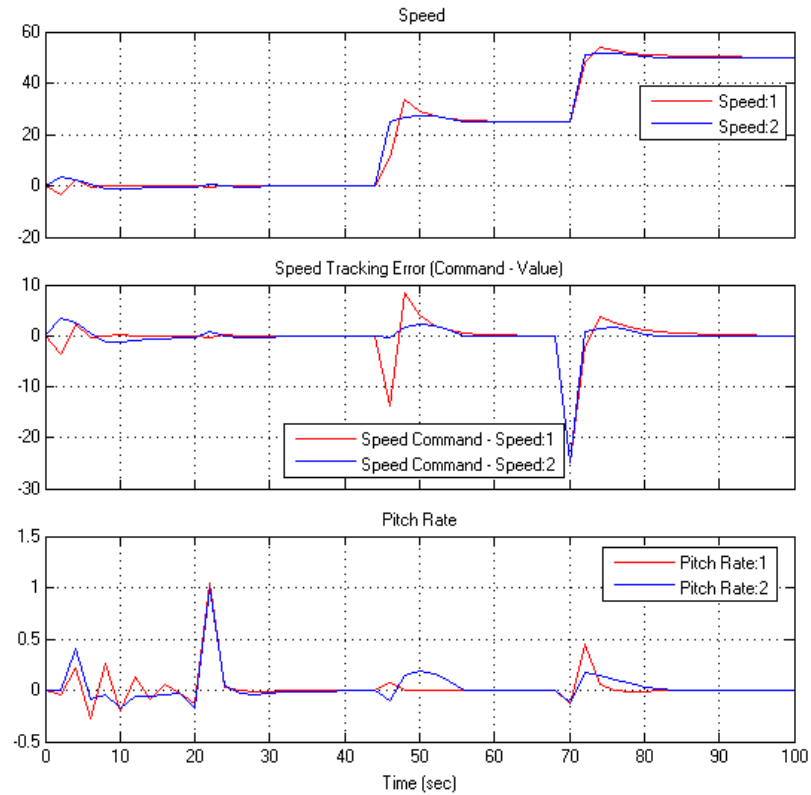


Figure 5.16: Speed, Speed tracking error and pitch rate (Red – SISO System, Blue – MIMO Case 1)

We see a faster speed tracking convergence, smaller overshoot and smaller speed tracking error for the MIMO case 1 when compared with SISO system (shown in Figure 5.16).

- For elevator maneuver, only the MIMO case 1 provides a better pitch rate response and better speed hold control.
- Although for speed command, input the SISO system provides much better pitch rate response but the MIMO case 1 control tracks speed more closely.
- For simultaneous elevator and speed, input the MIMO system provides a better pitch rate response and speed tracking.

Thus, in general the MIMO case 1 control setup performs comparatively better in all the aspects than the SISO control setup. In the next section, we summarize all the results in this report and share our future work ideas for the direct adaptive control scheme, multivariable systems, and hypersonic flight.

6. CONCLUSION AND FUTURE WORK

6.1 Summary

This thesis examines a high fidelity non-linear physic model of the hypersonic vehicle developed at the Air Force Research Lab, Wright-Patterson Air Force Base. The vehicle is characterized by unstable non-minimum phase dynamics with significant longitudinal coupling between fuel equivalency ratio and the angle of attack and the pitch angle. At high Mach number, the coupling between FER and FPA is increased. This coupling, inherent instability and non-minimum phase behavior create a need for control systems to provide augmented stability and control of the hypersonic vehicle.

In order to solve this problem we use a direct adaptive control scheme to design a stability and command augmentation system. The general mission profile was kept in consideration for this and the control system was designed in order to assist that mission goal. The pitch-axis stability augmentation is designed with the second control input set to a constant trim value. After successfully achieving an appropriate pitch rate response a second level of control system is added to track a speed command.

This work is followed by the multivariable direct adaptive approach. In this approach, the primary stability augmentation and secondary speed tracking control system is combined to study the advantages of the multivariable approach. It is observed that the multivariable HSV system possesses certain characteristics beneficial to the control scheme in terms of satisfying the stability theorem requirements. We also compare the performance of both control systems for a given set of commands.

6.2 Future Work

Apart from being longitudinally unstable, the X-51 hypersonic vehicle is also laterally unstable at both low and high speeds. At low speeds, the vehicle is directionally unstable for AoA less than 6 degrees and laterally unstable for AoA less than 2 degrees shown in Figure 6.1 and Figure 6.2 respectively. At high speeds, the vehicle is laterally unstable for AoA less than 9 degrees shown in Figure 6.3.

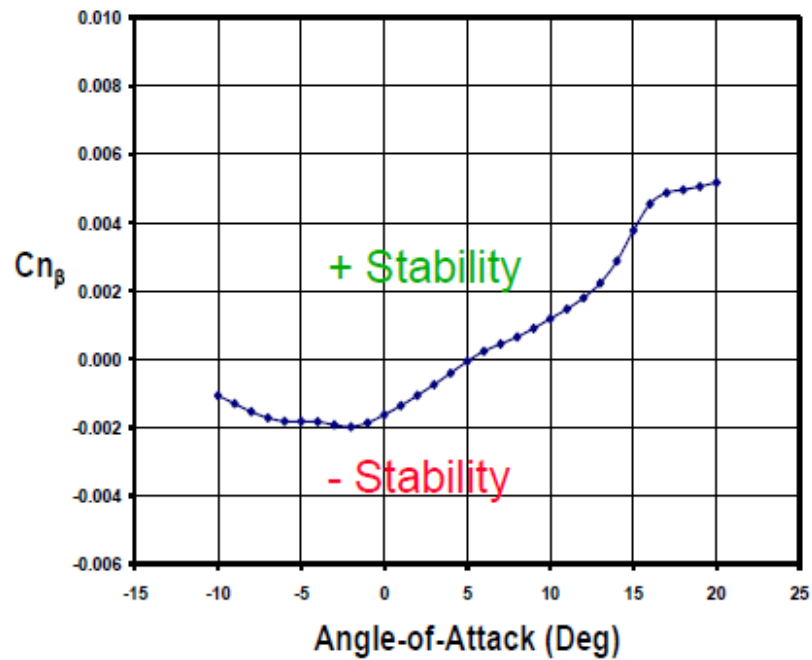


Figure 6.1: Directionally Unstable for AoA < 2 deg (Low Speed) (Mutzman, et al 2011)

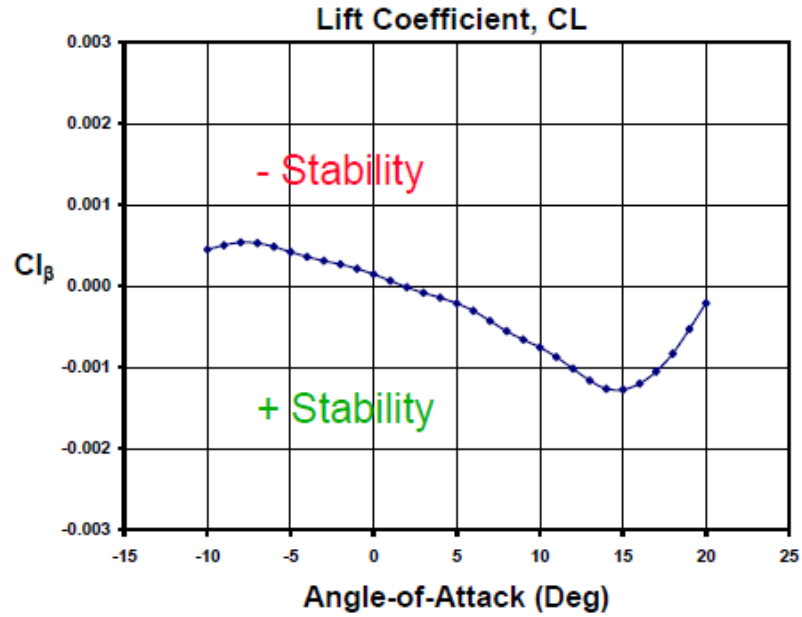


Figure 6.2: Laterally Unstable for AoA < 6 Deg (Low Speed) (Mutzman, et al 2011)

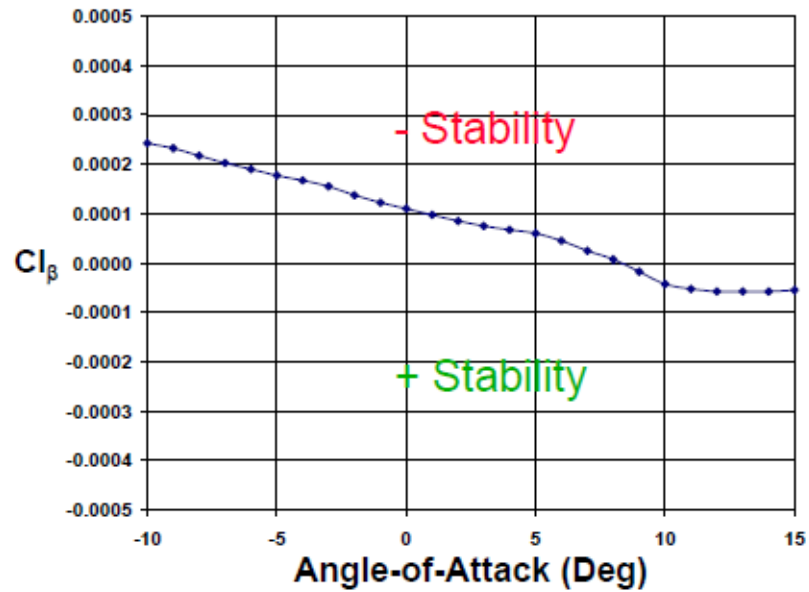


Figure 6.3: Laterally Unstable for AoA < 9 Deg (low Speed) (Mutzman, et al 2011)

With the control system designed in this work a third level lateral and directional stability augmentation system could be designed in order to achieve straight level flight on the 6-

DOF model. Once accomplished the direct adaptive control scheme could also be tested for the boosting phase. From boosting phase to cruising phase, the craft goes through a drastic change in weight, dimensions and parameters, posing a greater need for adaptivity on the control system.

7. REFERENCES

- Voland, R., Huebner L., and McClinton, C. (2005, October). X-43 Hypersonic Vehicle Technology Development. In 56th International Astronautical Congress of the International Astronautical Federation, the International Academy of Astronautics, and the International Institute of Space Law. Fukuoka, Japan.
- McClinton, C. R. (2006, January). X-43 Scramjet Power Breaks the Hypersonic Barrier Dryden Lectureship. Proceedings of 44th American Institute of Aeronautics and Astronautics Aerospace Sciences Meeting and Exhibit, Reno, Nevada.
- Bolender, M. A. (2009). An Overview on Dynamics and Controls Modelling of Hypersonic Vehicles. Proceedings of American Control Conference, St. Louis, MO.
- Bolender, M. A., and Doman, D. B. (2007). A Non-Linear Longitudinal Dynamical Model of a Hypersonic Vehicle. Journal of Spacecraft and Rockets, vol. 44, no. No. 2, pp. 374-387.
- Bolender, M., Oppenheimer, M. W., and Doman, D. B. (2007, August). Effects of unsteady and viscous aerodynamics on the dynamics of a flexible air-breathing hypersonic vehicle. Proceedings of American Institute of Aeronautics and Astronautics Atmospheric Flight Mechanics Conference and Exhibit, Hilton Head, South Carolina.
- Bolender, M. A., and Doman, D. B. (2006). Modeling Unsteady Heating Effects on the Structural Dynamics of a Hypersonic Vehicle. Proceedings of American Institute of Aeronautics and Astronautics Atmospheric Flight Mechanics Conference and Exhibit, Keystone, CO.
- Doman, D. B., and Bolender, M. A. (2006). An Aerothermal Flexible Mode Analysis of a Hypersonic Vehicle. Proceedings of American Institute of Aeronautics and Astronautics Atmospheric Flight Mechanics Conference and Exhibit, Keystone, CO.

- Oppenheimer, M. W., Skujins, T., Bolender, M. A., and Doman, D. B. (2007). A Flexible Hypersonic Vehicle Model Developed With Piston Theory. Proceedings of American Institute of Aeronautics and Astronautics Atmospheric Flight Mechanics Conference and Exhibit, Hilton Head, South Carolina.
- Cobleigh, B. R. (1998). Development of the X-33 Aerodynamic Uncertainty Model. NASA/TP-1998-206544, NASA Dryden Flight Research Center, CA.
- Stevens, B. L., and Lewis, F. L. (1992). Pitch-Axis Stability Augmentation. Aircraft Control and Simulation, Wiley-Interscience Publication, NY, NY. 237.
- Stevens, B. L., and Lewis, F. L. (2003). Aircraft Dynamics and Classical Control Design. Aircraft Control and Simulation, John Wiley and Sons, Hoboken, NJ. 292.
- Stevens, B. L., and Lewis, F. L. (1992). Stability Augmentation, in Aircraft Control and Simulation, Wiley-Interscience Publication, NY, NY. 238.
- Fuentes, R. J., and Balas, M. J. (2000, May). Direct Adaptive Rejection of Persistent Disturbances. Journal of Mathematical Analysis and Applications, vol. 251. 28-39.
- Balas, M. J., and Frost, S. A. (2013). Distributed Parameter Direct Adaptive Control Using a New Version of the Barbalat-Lyapunov Stability Result in Hilbert Space. Proceedings of American Institute of Aeronautics and Astronautics, Boston, MA.
- Balas, M. J., and Frost, S. A. (2014, July). Robust Adaptive Model Tracking for Distributed Parameter Control of Linear Infinite-Dimensional System in Hilbert Space. IEEE/CAA Journal of Automatica Sinica, vol. 1, no. No. 3.
- Balas, M. J., and Frost, S. A. (2016). A Zero Filter Augmentation for Robust Adaptive Control of Weakly Minimum Phase Finite-Dimensional Systems. Proceedings of American Institute of Aeronautics and Astronautics, SciTech, San Diego, California.
- Sigthorsson, D., Serrani, A., Yurkovich, S., Bolender, M., and Doman, D. (2006). Tracking control for an overactuated hypersonic air-breathing vehicle with steady state

constraints. Proceedings of American Institute of Aeronautics and Astronautics Guidance, Navigation and Control Conference, Keystone, CO, August.

Goodwin, G. C., and Sin, K. S. (1984) Adaptive Filtering Prediction and Control, Dover Publication, Inc.

Rausch, V. L., McClinton, C. R., and Crawford, J. L. (1997, Jan 01). Hyper-X: Flight Validation of Hypersonic Airbreathing Technology. Technical Report 20040110669, Aircraft Design, Testing AND Performance, NASA Langley Research Center, Hampton, VA, United States.

Letsinger J. M., (2012, Feb). Hypersonic Global Strike Feasibility and Options Thesis, USAF, Air War College, The Air University, Maxwell Air Force Base, Montgomery, Alabama.

V. M. Popov, V. M. (1973). Hyperstability of Control Systems. Springer-Verlag, Berlin.

Air Force Times. (2009, December). WaveRider Makes First Flight. Retrieved May 2015 from <http://archive.airforcetimes.com/article/20091222-/NEWS/912220334/WaveRider-makes-first-flight>

Villanueva R. (2007, June 01) Successful Design Review and Engine Test Bring Boeing X-51A Closer to Flight. Retrieved May 2015 from <http://boeing.mediaroom.com/2007-06-01-Successful-Design-Review-and-Engine-Test-Bring-Boeing-X-51A-Closer-to-Flight>

Wright-Patterson Air Force Base News (2010, May). X-51A flight planned May 25. Retrieved on May 2015 from <http://www.wpafb.af.mil/news-/story.asp?id=123205546>

Aseltine, J. A., Mancini, A. R., and Sartune, C. W. (1985). A survey of Adaptive Control Systems. IRE Transactions on Automatic Control, Vol. 3, no. 6. 102-108.

Caldwell, W.I., (1950). Control System with Automtic Response Adjustment. American patent, 2,517,081. Filed 25 April 1947.

- Hartmann, G. L., Barrett, M. F., and Greene, C. S. (1979, December). Control design for an unstable vehicle. NASA Dryden Flight Research Center, Contract Rep. NAS 4-257.
- Ngo, A. D., Reigelsperger, W. C., Banda, S. S., and Bessolo, J. S. (1996, July). Multivariable control law design of a tailless airplane. Proceedings of American Institute of Aeronautics and Astronautics paper 96-3866.
- Cameron, D., and Princen, N. (2000, August). Control allocation challenges and requirements for the Blended Wing Body. Proceedings of American Institute of Aeronautics and Astronautics Guidance, Navigation and Control Conference, American Institute of Aeronautics and Astronautics Paper 2000-4539.
- Friedmann, P. P. (1999, Jan – Feb). Renaissance of Aeroelastic and its Future. Journal of Aircraft, Vol. 36 No. 1.
- Bolender, M., and Doman, D. (2006). Flight Path Angle Dynamics of Air-Breathing Hypersonic Vehicles. Proceedings of American Institute of Aeronautics and Astronautics Guidance Navigation and Control Conf. and Exhibit, Paper No. 2006-6692, Tech. Rep.
- Nelson, R. C. (1998). Flight Stability and Automatic Controls, Second Ed., McGraw Hill.
- Balas, M. J. (2012, September 19 – 21). Adaptive Control of Nonminimum Phase Systems Using Sensor Blending With Application to Launch Vehicle Control. Proceedings of ASME 2012 Conference on Smart Materials, Adaptive Structure and Intelligent Systems, Vol 1, Stone Mountain, Georgia, USA.
- Wen, J. T. Y., and Balas, M. J. (1989). Robust Adaptive Control in Hilbert Space. Journal of Mathematical Analysis and Applications.
- Ioannou, P. A., and Sun, J. (2012). Robust Adaptive Control, Dover Publication, Inc.
- Hespanha, J. P. (2009) Linear Systems Theory, Princeton University Press, 167-176.

- Osburn, P. V., Whitaker, A. P., and Kezer, A. (1961). New Developments in the Design of Model Reference Adaptive Control Systems. Paper No. 61-39, Institute of the Aerospace Sciences.
- Whitaker, A. P., Yamron, J., and Kezer, A. (1958). Design of Model Reference Adaptive Control Systems for Aircraft. Report R-164, Instrumentation Laboratory, M. I. T. Press, Cambridge, Massachusetts.
- Tsytkin, Y. Z. (1971). Adaptation and Learning in Automatic Systems, Academic Press, New York.
- Harris, C. J., and Billings, S. A. (1981). (Eds), Self-Tuning and Adaptive Control: Theory and Applications, Peter Peregrinus, London.
- Unbehauen, H. (1980). (Ed.) Methods and Applications in Adaptive Control, Springer-Verlag, Berlin.
- Åström†, K. J., and Wittenmark, B. (1989). Adaptive Control, Addison-Wesley Publishing Company, Reading, Massachusetts.
- Chalam, V. V. (1987). Adaptive Control Systems: Techniques and Applications, Marcel Dekker, New York.
- Egardt, B. (1979). Stability of Adaptive Controllers, Lecture Notes in Control and Information Sciences, Vol. 20, Springer-Verlag, Berlin.
- Ioannou, P. A., and Sun, J. (2012). Robust Adaptive Control, Dover Publication, Inc. 12-33.
- Narendra, K. S., and Annaswamy, A. M. (2005). Stable Adaptive Systems, Dover Publications, Inc., 1 – 41.
- Narendra, K. S., Tripathi, S. S., Luders, G., and Kudva, P. (1971, October). Adaptive control using Lyapunov's direct method. Technical Report No. CT-43, Becton Center, Yale University, New Haven, CT.

- Wen, J. (1985, June). Direct Adaptive Control in Hilbert Space. Ph.D. thesis, Electrical, Computer and Systems Engineering Department, Rensselaer Polytechnic Institute, Troy, NJ.
- Balas, M., and Fuentes, R. (2004). A Non-Orthogonal Projection Approach to Characterization of Almost Positive Real Systems with an Application to Adaptive Control. Proceedings of American Control Conference.
- Ioannou, P. A., and Sun, J. (2012). Robust Adaptive Control, Dover Publication, Inc. 10 – 11.
- Balas, M., Gajendar, S., and Robertson, L. (2009, August). Adaptive Tracking Control of Linear Systems with Unknown Delays and Persistent Disturbances (or Who You Callin' Retarded?). Proceedings of the American Institute of Aeronautics and Astronautics, Guidance, Navigation and Control Conference, Chicago, IL.
- Balas, M., Magar, K. T., and Frost, S. (2012). Large Wind Turbine in Variable Speed Transition Operation: Adaptive Disturbance Tracking Control. Proceedings of American Institute of Aeronautics and Astronautics InfoTech@ Aerospace Conference.
- Balas, M., Magar, K. T., and Frost, S. (2012). Adaptive Disturbance Tracking theory with state estimation and state feedback for region II control of large wind turbines. American Control Conference (ACC), IEEE.
- Schlipf, D., et. al. (2013). Nonlinear model predictive control of floating wind turbines. The Twenty-third International Offshore and Polar Engineering Conference. International Society of Offshore and Polar Engineers.
- Li, N., and Balas, M. J. (2014, June 4 – 6). Direct Periodic Adaptive Control of the aerodynamic loads of a rotating wind turbine blade using microtabs. Proceedings of American Control Conference (ACC), vol., no., 4428-4433.

- Parker, J. T., Serrani, A., Yurkovich, S., Bolender, M., and Doman, D. (2007, May – June). Control-Oriented Modeling of an air-breathing hypersonic vehicle. *Journal of Guidance, Control, and Dynamics*, 30(3).
- Anderson, J. (2006). *Hypersonic and High-Temperature Gas Dynamics*, Second Edition. American Institute of Aeronautics and Astronautics, 225.
- Skogestad, S., and Postlethwaite, I. (2005). *Multivariable Feedback Control Analysis and Design*, John Wiley and Sons, Ltd 65 – 117.
- Skogestad, S., and Postlethwaite, I. (2005). *Multivariable Feedback Control Analysis and Design*, John Wiley and Sons, Ltd, 2005, 67 – 68.
- Skogestad, S., and Postlethwaite, I. (2005). *Multivariable Feedback Control Analysis and Design*, John Wiley and Sons, Ltd, 2005, 96 – 98.
- Balas, M., Fuentes, R., and Mehie, E. (2003). Adaptive Control and Rejection of Persistent Disturbance: Continuous and Discrete-Time. In *Proceedings of American Institute of Aeronautics and Astronautics-Guidance, Navigation and Control Conference*.
- Hartman, A. (2011). *Adaptive Control of Nonminimum Phase Systems Using Sensor Blending with Application to Launch Vehicle Control*. Thesis, University of Wyoming.
- Korad, A. (2010, May). *Modeling, Analysis, and Control of a Hypersonic Vehicle with Significant Aero-Thermo-Elastic-Propulsion Interactions, and Propulsive Uncertainty*. Master's Thesis, Arizona State University, Tempe, AZ.
- Mutzman, R., and Murphy, S. (2011). 'X-51 Development: A Chief Engineer's Perspective'. Presentation.